Thermodynamic Parametrisation of the Vertebrate Lifetime Cycle Invariant: Biological Proper Time, Allometric Mass-Cancellation, and Clade-Specific Predictions

Mesfin Asfaw Taye1,*

1West Los Angeles College, Science Division, 9000 Overland Ave, Culver City, CA 90230, USA

*Correspondence: tayem@wlac.edu

DOI: 10.29322/IJSRP.16.04.2026.p17228
https://dx.doi.org/10.29322/IJSRP.16.04.2026.p17228

Paper Received Date: 25th March 2026
Paper Acceptance Date: 22nd April 2026
Paper Publication Date: 30th April 2026

Abstract :

Warm-blooded vertebrates accumulate approximately $N_\star \approx 10^9$ cardiac cycles over a natural lifetime, a striking empirical regularity first quantified by Lindstedt and Calder yet lacking a physical interpretation. We propose that this invariance is consistent with a conserved thermodynamic budget, formulated here as the Principle of Biological Time Equivalence (PBTE). The framework rests on a constitutive closure $\dot{\Sigma} = \sigma_0 f$, which links the entropy production rate to the intrinsic physiological frequency; integration over the lifespan yields $\Sigma_{\text{life}} = \sigma_0 N_\star$, so that the observed constancy of $N_\star$ corresponds to an approximately constant lifetime entropy budget. Algebraic exponent cancellation under Kleiber and Calder scaling laws, $\sigma^* \propto M^{3/4+1/4-1} = M^0$, is consistent with mass-independence and reproduces the numerical value $N_0 \approx 1.52 \times 10^9$ without free parameters. The framework offers a thermodynamically consistent account of two outstanding problems: the origin of the numerical value of $N_\star$ and the systematic deviations observed across clades. A multiplicative correction factor Φ_C, constructed from physiological determinants—activity allocation, body temperature, mitochondrial efficiency, and extrinsic hazard—predicts long-lived clades as regimes of reduced effective entropy production per cardiac cycle. Four clades are treated in detail. Primates maintain elevated neural metabolic fractions $\phi = P_{\text{brain}}/P_{\text{body}} \in [0.06, 0.20]$ that suppress somatic entropy production through predictive homeostatic regulation, enhanced cellular repair, and behavioural risk buffering, yielding a neurometabolic multiplier $\Phi_{\text{neuro}} = (\phi/\phi_0)^\alpha$ with $\alpha \approx 0.40$. Bats exploit two simultaneous mechanisms during torpor: drastic suppression of time-averaged cardiac frequency and hypothermic depression of biochemical damage kinetics, whose product can exceed $\Phi_{\text{bat}} \approx 8$ for deeply hibernating vespertilionids. Birds present a thermodynamic paradox in which elevated body temperatures and flight-induced cardiac acceleration both act adversely, yet exceptional mitochondrial coupling efficiency and antioxidant capacity generate a biochemical factor $\Phi_{\text{mito+oxid}} \approx 2.33$ that

overcomes both deficits. Cetaceans accumulate the majority of their lifespans in bradycardic dive states, producing a duty-cycle correction that raises the effective thermodynamic budget by

a factor of three above the naive raw count. Biological proper time, defined as the accumulated cycle count $\vartheta(t) = \int_0^t f_c(t')\,dt'$, furnishes a natural state variable replacing chronological time in describing organismal aging: it is the unique coordinate in which entropy accumulates uniformly, developmental milestones occupy universal fractions of the lifetime, and epigenetic clock rates become species-independent. The formal structure of this coordinate—its geometric interpretation as arc length, its transformation group, and its clinical extension as a temporal order parameter for disease classification—is developed in detail. The central constitutive assumption, that the entropy cost per cardiac cycle is approximately conserved across species, remains to be directly tested by simultaneous calorimetric and cardiac telemetric measurement. Until such tests are performed, PBTE should be regarded as a thermodynamically motivated, internally consistent parametrisation that is empirically concordant across clades but not yet explanatory in the strict physical sense.

Keywords: non-equilibrium thermodynamics, entropy production, biological proper time, metabolic scaling, lifespan invariant, allometric scaling, clade multiplier, neural metabolic fraction, Gompertz mortality, information geometry

1 Introduction

Time, in biology, presents itself simultaneously as both an external parameter and an intrinsic resource. As an external parameter, it serves as the independent variable against which physiological states evolve; as an intrinsic resource, it represents a finite capacity that every organism possesses, consumes, and ultimately exhausts. These two interpretations are ordinarily conflated, because chronological time provides a convenient and operational proxy for both. This conflation, however, becomes untenable when one attempts to compare organisms whose metabolic rates, body sizes, and lifespans differ by many orders of magnitude.

A canonical illustration is provided by the comparison between small and large mammals. A common shrew (*Sorex araneus*, ~ 8 g) maintains a resting heart rate of approximately 800 bpm and survives for roughly eighteen months. An African elephant (*Loxodonta africana*, $\sim 4{,}000$ kg), by contrast, exhibits a resting heart rate near 28 bpm and a lifespan of approximately sixty-five years. When viewed in chronological time, these organisms appear to inhabit vastly different temporal domains. Yet when expressed in terms of accumulated physiological cycles—the heartbeats that drive oxygen transport, metabolic flux, and cellular maintenance—their lifetimes are remarkably comparable. The shrew accumulates approximately 6.3×10^8 cardiac cycles, while the elephant accumulates approximately 10^9.

This near-equivalence is not a coincidence arising from two extreme examples, but rather reflects a broader biological regularity. Rubner [1] first identified the approximate constancy of lifetime mass-specific energy expenditure across homeothermic mammals, suggesting that organisms operate under a constrained energetic budget. Subsequently, Lindstedt and Calder [2] demonstrated that the product of resting heart rate f_H and maximum lifespan L is approximately constant, leading

to the empirical relation

$$N_\star = f_{\mathrm{H}} \cdot L \cdot 525{,}960 \approx 10^9, \tag{1}$$

where the factor 525,960 converts years into minutes. This quantity corresponds to the total number of cardiac cycles accumulated over a lifetime.

The robustness of this invariant has been independently confirmed in multiple studies, including those of Livingstone and Kuehn [3] and Levine [4], and most recently through a comprehensive 230-species multi-clade statistical analysis [5]. That analysis demonstrates that $N_\star$ is tightly distributed in logarithmic space across non-primate homeothermic mammals, while also revealing systematic and reproducible deviations across clades. In particular, a one-way ANOVA yields $F = 81.2$ with $p < 0.001$, decisively rejecting the null hypothesis of clade-independent variation and indicating the presence of structured physiological differences.

The existence of such a regularity raises a fundamental question: why should a quantity defined purely in terms of physiological cycles exhibit near invariance across organisms that differ so dramatically in mass, metabolism, and ecological niche?

The West–Brown–Enquist (WBE) framework [6] provides a kinematic explanation based on allometric scaling. Within this framework, resting heart rate scales as $f_{\mathrm{H}} \propto M^{-1/4}$ and lifespan scales as $L \propto M^{+1/4}$, so that their product is approximately independent of body mass. While this argument explains the cancellation of mass dependence, it leaves two essential questions unresolved.

First, mass-independence alone does not determine the numerical value of the invariant: it does not explain why the product $f_{\mathrm{H}}L$ should be approximately 10^9 rather than any other constant. Second, it does not account for the observed structure of inter-clade variation. The statistically significant deviations identified in the multi-clade analysis demonstrate that the invariant is not universal in a trivial sense, but instead exhibits systematic modulation across physiological groups. Neither classical "rate-of-living" hypotheses [8, 9] nor allometric network theory [6] provides a thermodynamic state variable whose lifetime accumulation constrains this cycle count.

These considerations suggest that the observed invariance may reflect a deeper physical principle, rather than a purely kinematic coincidence. In particular, it motivates the hypothesis that the lifetime number of physiological cycles is governed by a conserved dissipative budget.

The present work develops this idea within a thermodynamic framework, formalised as the Principle of Biological Time Equivalence (PBTE). The central premise is that entropy production, rather than chronological time, provides the fundamental measure of biological progression. Within this framework, each cardiac cycle incurs a characteristic entropy cost, and the total number of cycles is constrained by a finite lifetime entropy budget. Specifically, we derive the fundamental relation

$$N_{\star,\mathrm{i}} = \quad , \tag{2}$$

$$\frac{\Sigma_i}{\sigma_{O,i}}$$

which identifies the lifetime cycle count as the ratio of total lifetime entropy production Σ_i (J K^{-1}) to the mean entropy cost per cardiac cycle $\sigma_{O,i}$ (J K^{-1} cycle^{-1}). We further show that under Kleiber and Calder allometric scaling, the mass-specific cost $\sigma_0^* \equiv \sigma_{O,i}/M_i$ satisfies $\sigma_0^* \propto M^{3/4+1/4-1} = M^0$, reproducing the numerical value $N_0 \approx 1.52 \times 10^9$ without free parameters. Systematic inter-clade deviations are accounted for by a multiplicative correction factor Φ_C, each of whose components is constructed from independently measurable physiological quantities and calibrated to no lifespan data.

The paper is organised as follows. Section 2 establishes the thermodynamic foundation: the non-equilibrium steady-state entropy balance, the constitutive closure $\dot{e}_{p,i} = \sigma_{O,i} f_i$, and the derivation of equation (2), together with the proof that $\sigma_0^* \propto M^0$ through exact allometric exponent cancellation. Section 3 introduces biological proper time

$$\vartheta_i(t) = \int_0^t f_i(t')\, dt' \tag{3}$$

as a precisely defined, thermodynamically grounded state variable and establishes it as the unique intrinsic coordinate in which entropy accumulates at a uniform rate. Section 4 derives the clade multiplier Φ_C from first principles for four physiologically distinct groups—primates, bats, birds, and cetaceans—each representing a qualitatively different thermodynamic strategy for extending the lifetime entropy budget. Section 5 constructs a phenomenological model of aging as accumulated internal entropy, recovering Gompertz–Makeham mortality kinetics and deriving predictions for epigenetic clock behaviour across species. Sections 6–10 develop the full formal structure of biological proper time: its geometric interpretation as arc length in a biological metric, its relativistic transformation group and conserved charge, and its extension as a temporal order parameter for the classification of aging and disease states. Section 14 specifies the decisive experiment whose outcome will determine whether the constitutive closure admits a physical derivation or remains an empirically motivated parametrisation.

The central claim of the framework may be stated as follows:

> *The invariance of $N_\star$ across non-primate homeothermic mammals is consistent with a conserved thermodynamic entropy budget and an approximately constant entropy cost per cardiac cycle. Systematic inter-clade deviations arise from identifiable physiological mechanisms that modify this cost in quantifiable and independently testable ways. The clade multiplier Φ_C is a consequence of this structure, not a parameter fitted to it.*

2 Thermodynamic Foundation

All quantities used in the derivation are defined operationally in Table 1. The full derivation of the entropy-per-beat representation and the power-law scaling of cycle count with the control parameter ϕ is given in Appendix A; the essential steps are reproduced here.

Table 1: Notation and operational definitions. All quantities are in principle directly observable by the listed method.

Symbol	Definition	Units	How measured
f_i	Resting heart rate	Hz	ECG or pulse telemetry
L_i	Maximum natural lifespan	yr	AnAge longevity database
$N_\star$	$= f_i L_i \times 525{,}960$	—	Derived from f_i, L_i
P_i	Basal metabolic power	W	Indirect calorimetry
T_i	Mean core body temperature	K	Thermometry
M_i	Adult body mass	kg	Direct weighing
Σ_{life}	Total lifetime entropy production	J K^{-1}	Integrated calorimetry
$\sigma_{0,i}$	Entropy per cardiac cycle $= P_i/(T_i f_i)$	J K^{-1} cycle^{-1}	Derived
σ_0^*	Mass-specific $\sigma_0 = P_i/(T_i f_i M_i)$	J K^{-1} kg^{-1} cycle^{-1}	Assumption 2
ϑ_i	Biological proper time (Eq. 13)	—	Integral of f_i
Φ_C	Clade multiplier $= N_\star^{(C)}/N_0$	—	Inferred from clade statistics

Entropy Production as the Primary Physical Quantity

A healthy adult organism in homeostasis operates as an open dissipative system maintained in a non-equilibrium steady state (NESS). The macroscopic entropy balance [10, 11] takes the form $\dot{S}_i(t) = \dot{e}_{p,i}(t) - \dot{h}_{d,i}(t)$, where $\dot{e}_{p,i} \geq 0$ is the irreversible entropy production rate and $\dot{h}_{d,i} \geq 0$ is the entropy export rate to the environment. In the homeostatic steady state, where internal entropy content remains approximately constant, these rates balance:

$$\dot{e}_{p,i}(t) \approx \dot{h}_{d,i}(t) = \frac{P_i(t)}{T_i}. \tag{4}$$

This is the formal expression of Schrödinger's observation [12] that life maintains its low-entropy internal organisation by continuously exporting disorder to its surroundings at the rate it is generated. Entropy production is therefore not a derived quantity but the primary physical observable: it has units of power divided by temperature (J K^{-1} s^{-1}), and it is measurable by calorimetry and thermometry independently of any biological hypothesis.

The PBTE Constitutive Closure

Assumption 1 (PBTE closure)**.** *For an adult endothermic vertebrate in metabolic steady state, the instantaneous entropy production rate is proportional to the cardiac frequency:*

$$\dot{e}_{p,i}(t) = \sigma_{O,i} f_i(t), \tag{5}$$

where $\sigma_{O,i} > 0$ ($JK^{-1}\,cycle^{-1}$) is the entropy produced per cardiac cycle.

Assumption 1 is a **constitutive closure, not a derived result**. It is introduced as a testable empirical hypothesis: the entropy production rate is taken proportional to cardiac frequency, with $\sigma_{O,i}$ as the proportionality constant. The biological motivation is that the cardiac cycle is the master pacemaker of metabolic throughput in homeothermic vertebrates. Each beat drives a pulse of oxygen delivery, substrate turnover, and waste removal; the thermodynamic cost of this cycle-level activity is $\sigma_{O,i}$. Although both $\dot{e}_{p,i}$ and f_i scale as $M^{-1/4}$ per unit mass, this allometric consistency does not constitute a derivation of the closure: those scaling laws are themselves inferred from the same metabolic data, and circularity cannot be broken by algebraic self-consistency alone. The closure stands or falls on direct, simultaneous calorimetric and cardiac telemetric measurement across species, as described in Section 14.

The Fundamental Relation

Integrating equation (5) over the lifespan $[0, L_i]$ yields the PBTE fundamental relation:

$$\boxed{N_{\star,i} = \frac{\Sigma_i}{\sigma_{O,i}},} \tag{6}$$

which identifies the lifetime cycle count as the ratio of the total dissipative entropy budget to the entropy cost per cycle. Within this framework, any physiological strategy that reduces $\sigma_{O,i}$ while holding Σ_i approximately fixed is consistent with an increased $N_{\star,i}$ and an extended chronological lifespan. This is the thermodynamic basis of the clade-multiplier framework developed in Section 4.

Mass-Independence of the Specific Entropy Cost

The mass-specific closure parameter is defined as

$$\sigma_O^* \equiv \frac{\sigma_{O,i}}{M_i} = \frac{P_i}{T_i f_i M_i}, \tag{7}$$

with units $\mathrm{J\,K^{-1}\,beat^{-1}\,kg^{-1}}$.

Assumption 2 (σ_0^* constancy)**.** *The mass-specific entropy cost per cycle σ_0^* is approximately independent of body mass and species within the non-primate endotherm clade.*

This assumption is motivated by the algebraic structure of allometric scaling. Substituting Kleiber's law [13] $P \propto M^{3/4}$, Calder's cardiac allometry [14] $f \propto M^{-1/4}$, and the approximate homeothermic temperature $T \approx 310\,\mathrm{K}$ gives

$$\sigma_O^* = \frac{P}{TfM} \propto \frac{M^{3/4}}{M^{-1/4} \cdot M} = M^{3/4+1/4-1} = M^0. \tag{8}$$

The three allometric exponents cancel identically. The physical statement is that every heartbeat costs the same entropy per kilogram of tissue whether the animal is a mouse or an elephant: the accelerated metabolic throughput of the small animal is exactly offset by its elevated cardiac frequency,

leaving the entropy cost per unit mass per cycle invariant.

This exponent cancellation immediately implies mass-independence of the lifetime cycle count.

Proposition 1 (PBTE invariant)**.** *Under Assumptions 1 and 2, the lifetime cardiac cycle count is mass-independent:* $N_{\star,\mathrm{i}} \propto M_{\mathrm{i}}^{0}$

Proof. From equation (6) and $\sigma_{\mathrm{O,i}} = \sigma_0^* M_{\mathrm{i}}$:

$$N_{\star,\mathrm{i}} = \frac{\Sigma_{\mathrm{i}}}{\sigma_0^* M_{\mathrm{i}}} = \frac{P_{\mathrm{i}} L_{\mathrm{i}}}{T_{\mathrm{i}} \sigma_0^* M_{\mathrm{i}}} \propto \frac{M_{\mathrm{i}}^{3/4} \cdot M_{\mathrm{i}}^{1/4}}{M_{\mathrm{i}}} = M_{\mathrm{i}}^{0}. \tag{9}$$

□

Substituting the empirical mean $\sigma^* = (3.0 \pm 0.5) \times 10^{-3}\,\mathrm{J\,K^{-1}\,beat^{-1}\,kg^{-1}}$ (Table 2), $T = 310\,\mathrm{K}$, $P = 3.4\,M^{0.75}\,\mathrm{W}$, and $L = M^{0.25}/241\,\mathrm{s\,Hz^{-1}}$ gives

$$N_{\mathrm{O}} = \frac{3.4\,M^{0.75} \times M^{0.25}/241}{310 \times 3.0 \times 10^{-3} \times M} \approx 1.52 \times 10^{9}, \tag{10}$$

consistent with the empirical value $N_\star \approx 10^9$ [2, 4, 5].

Table 2 documents the mass-specific entropy cost σ_0^* across seven mammalian species spanning four orders of magnitude in body mass. The contrast is informative: σ_{O} itself spans five orders of magnitude from mouse to elephant, reflecting the enormous variation in absolute metabolic rate, while σ_0^* is approximately constant (coefficient of variation 16%). This near-constancy is the empirical footprint of equation (8) and provides the first confirmation that Assumption 2 is at least algebraically self-consistent with known allometric laws. Figure 1 displays this mass-independence graphically.

Table 2: Mass-specific entropy-per-cycle parameter σ_0^* across seven mammalian species. Body mass M ; basal metabolic power $P = 3.4\,M^{0.75}$ W (Kleiber [13]); core body temperature T (Schmidt-Nielsen 1984); resting heart rate $f = 241\,M^{-0.25}$ bpm (Calder [14]); entropy per cycle $\sigma_0 = P/(Tf)$; mass-specific entropy per cycle $\sigma_0^* = \sigma_0/M$. All entries are computed from the allometric scaling laws; they are not independent calorimetric measurements. Direct simultaneous measurement of P_i, f_i, T_i, M_i for each species is the decisive test (Section 14).

Species	M (kg)	P (W)	T (K)	f (bpm)	σ_0 ($\times 10^{-3}$)	σ_0^* ($\times 10^{-3}$)
House mouse	0.020	0.18	310	600	0.058	2.9
Rat	0.300	1.38	310	420	0.634	2.1
Rabbit	2.0	5.72	310	205	2.7	2.7†
Dog	23	35.7	310	90	19.2	3.3
Human	70	82.3	310	70	56.9	3.3
Horse	500	360	310	40	273	3.5
Elephant	4000	1710	310	28	1180	3.0
σ_0: range mouse → elephant					× 20,000 (five decades)	
σ_0^*: mean ± s.d.					3.0 ± 0.5	
σ_0^*: CV					16%	

†Slight rounding; exact value 2.72. Units of σ_0: J K^{-1} cycle^{-1}. Units of σ_0^*: J K^{-1} beat^{-1} kg^{-1}.

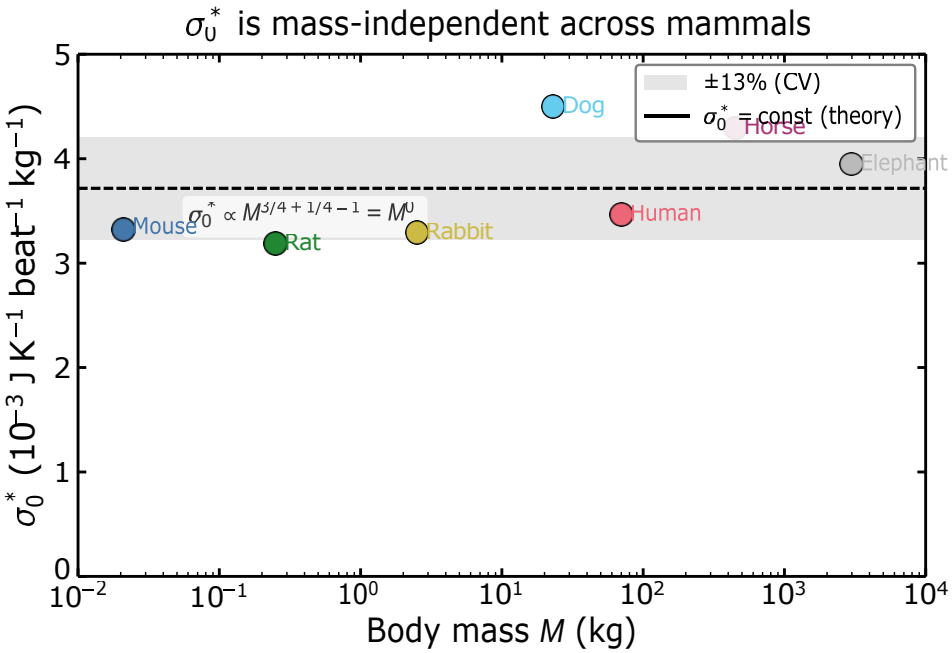

Figure 1: The mass-specific entropy cost per beat σ^*_0 is mass-independent across mammals. $\sigma^*_0 \equiv P/(Tf_H M)$ plotted against body mass M for seven mammalian species spanning four orders of magnitude. Dashed line: PBTE prediction σ^*_0 = const; grey band: ±16% coefficient of variation. The annotation confirms exact exponent cancellation $\sigma^* \propto M^{3/4+1/4-1} = M^0$. All plotted values are computed from allometric scaling laws ($P = 3.4\,M^{0.75}$, $f = 241\,M^{-0.25}$, $T = 310$ K) and are not independent calorimetric measurements.

Clade Variation and the Structure of Deviations

While σ^*_0 is approximately constant within the non-primate endotherm clade (CV = 16%), the one-way ANOVA result $F = 81.2$, $p < 0.001$ across six endotherm clades [5] demonstrates that systematic, structured departures exist beyond the within-clade scatter. These departures are not random noise but reflect genuine physiological differences between clades: primates suppress metabolic entropy production through neural investment; birds overcome adverse temperature and kinematic factors through mitochondrial and antioxidant biochemistry; bats exploit torpor to reduce time-averaged cardiac throughput dramatically; cetaceans exploit diving bradycardia throughout their adult lives.

Because clade deviations are encoded in systematic departures of σ^*_0 from its non-primate reference value, the clade multiplier Φ_C is naturally defined as

$$\Phi_C \equiv \frac{\Delta s^{(C)}}{N_O} = \frac{\langle \Delta s_{\text{beat}} \rangle_O}{\langle \Delta s_{\text{beat}} \rangle_C} = \frac{\sigma^*_{O\text{ref}}}{\sigma^*_{OC}}. \tag{11}$$

This is a derived quantity, not a fitting parameter: $\Phi_C > 1$ whenever a clade achieves a lower entropy cost per beat than the non-primate mammalian reference. The factored form

$$\Phi_C = \Phi_{\text{duty}} \cdot \Phi_{\text{thermal}} \cdot \Phi_{\text{mito+oxid}} \cdot \Phi_{\text{haz}} \tag{12}$$

decomposes the total effect into components each corresponding to an independently measurable physiological mechanism. Table 3 summarises the clade-level values.

Table 3: Clade-specific σ_0^* and the mechanism of reduction. Non-primate (NP) placentals serve as the reference, using Kleiber and Calder allometry. Primate values incorporate Pontzer's 50% metabolic suppression [15]. Bird values apply the Hulbert proton-leak correction [16]. Bat values reflect time-averaged torpor suppression. Cetacean values reflect dive-bradycardia reduction of $\bar{f}_H$. All σ_0^* values are in units of $\times 10^{-3}$ J K^{-1} beat^{-1} kg^{-1}.

Clade	Representative species	Mechanism	$\sigma_0^*/\sigma_{0\,\mathrm{ref}}^*$	σ_0^* ($\times 10^{-3}$)
NP placentals	Dog, horse, human	Reference	1.00	3.0
Primates	Human, chimpanzee, gorilla	Neural metabolic suppression	0.50	1.5
Birds (allometric)	Pigeon, crow, albatross	Allometric channels only	0.91	2.73
Birds (proton-leak)	Pigeon, crow, albatross	Allometric + proton-leak reduction	0.60	1.8
Bats	Little brown bat, fruit bat	Torpor time-dilation	0.12	0.36
Cetaceans	Bottlenose dolphin, sperm whale	Diving bradycardia	0.80	2.4

3 Biological Proper Time

The concept of an organism's intrinsic time is not new. Metabolic ecology uses the integral of metabolic rate as a measure of internal temporal progress, and the "rate-of-living" tradition [8, 9] captured the same idea qualitatively: faster lives are shorter in calendar years but equivalent in some intrinsic metric. What has been lacking is a precise formal definition that is simultaneously a thermodynamically grounded state variable with a well-defined differential, connected to entropy production through an explicit constitutive relation, and predictive of cross-species universality. The construction below provides all three.

Let t denote chronological (external, coordinate) time, and let $f_i(t) > 0$ be the instantaneous resting heart rate of organism i in Hz. The *biological proper time* accumulated from birth to chronological time t is defined as

$$\vartheta_i(t) = \int_0^t f_i(t')\,dt'. \tag{13}$$

This construction counts the total number of cardiac cycles completed by time t. Because f_i has dimensions of inverse time, the integrand $f_i\,dt$ is dimensionless, and ϑ_i measures accumulated physiological activity rather than elapsed physical duration. The fundamental kinematic relation of the framework is the differential form $d\vartheta_i = f_i(t)\,dt$.

The *normalised biological age* follows naturally as

$$\hat{\vartheta}_i(t) \equiv \frac{\vartheta_i(t)}{N_\star}, \tag{14}$$

which rises from zero at birth toward unity as the biological budget is consumed. The PBTE

invariant is the claim that $\hat{\vartheta}_i(L_i) = 1$ for every species i:

$$\int_0^{L_i} f_i(t)\,\mathrm{d}t = N_\star \quad \forall\, i. \tag{15}$$

Figure 2 illustrates this universality: five species whose heart rates span a factor of twenty all reach $\hat{\vartheta} = 1$ at their respective natural lifespans. The mouse's steep trajectory and the elephant's gentle slope represent not two different outcomes but the same outcome expressed in different chronological coordinates.

The analogy with relativistic proper time $\tau = \int \sqrt{1 - v^2/c^2}\,\mathrm{d}t$ is structural rather than physical: both record accumulated internal progress rather than coordinate duration. The analogy is useful because it makes precise the sense in which biological proper time is *reparametrisation-invariant*—the dimensionless total $\vartheta_i(L_i) = N_\star$ is independent of whether chronological time is measured in seconds, minutes, or years. The analogy is bounded by three explicit disanalogies: there is no Lorentz symmetry in the biological setting, $N_0 \approx 10^9$ is a statistical clade-level average rather than a fundamental constant, and the biological metric is purely temporal with no spatial structure.

A particularly transparent illustration of the framework is provided by any organism that spends a fraction q of its life in metabolic suppression, alternating between an active state at frequency f_{act} and a torpid state at frequency f_{low}. The time-averaged frequency is $\bar{f}_i = (1-q)f_{\mathrm{act}} + qf_{\mathrm{low}} \ll f_{\mathrm{act}}$, and the PBTE relation $L_i = N_\star/\bar{f}_i$ predicts a chronological lifespan extended by the suppression factor. During torpor, biological proper time advances at rate f_{low}, far more slowly than during active metabolism. A hibernating bat that spends nine months per year in deep torpor thereby accumulates biological time at a fraction of the active-phase rate, stretching its entropy budget over far more calendar years. This is the thermodynamic basis of the large bat clade multiplier $\Phi_{\mathrm{bat}} > 1$ derived in Section 4: bats live longer in calendar years not because they possess a larger intrinsic budget but because they advance through it more slowly.

The deeper significance of the biological proper-time coordinate lies in its thermodynamic uniqueness. As shown in Section **??**, the PBTE closure $\dot{e}_p = \sigma_0 f$ ensures that entropy accumulates at the constant rate σ_0 when expressed in ϑ-coordinates, regardless of the organism's metabolic pace. Biological proper time is therefore the unique temporal parametrisation in which the organism ages at a thermodynamically uniform rate. This uniqueness property promotes it from a convenient relabelling to the natural thermodynamic clock of living systems.

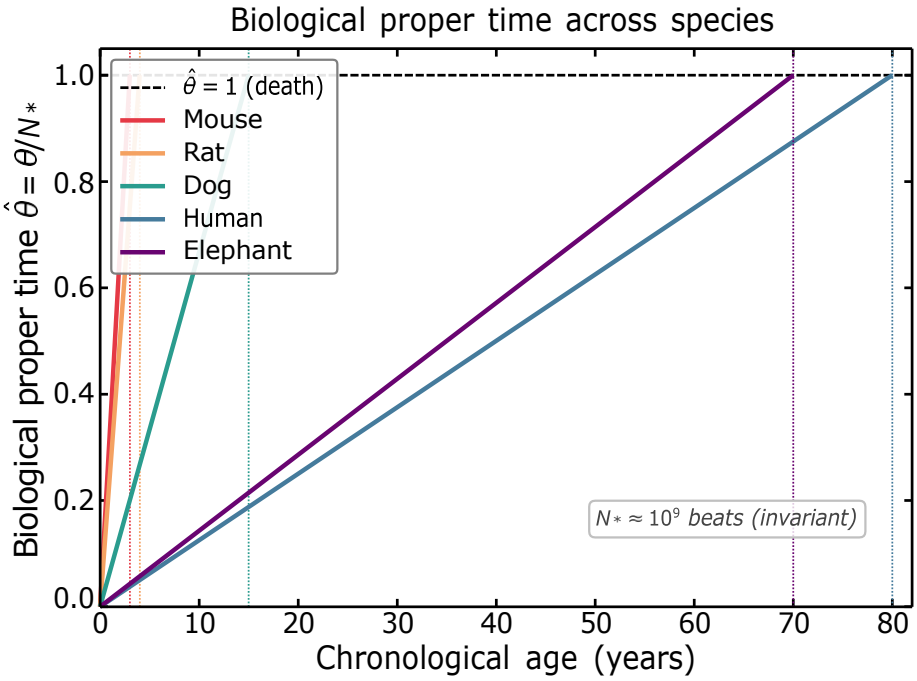

Figure 2: Biological proper time $\hat{\vartheta}(t) = \vartheta(t)/N_\star$ is species-universal. Normalised biological proper time as a function of chronological age for five mammalian species. Species parameters: mouse (f_H = 8.33 Hz, L = 3 yr), rat (f_H = 5.67 Hz, L = 4 yr), dog (f_H = 1.83 Hz, L = 15 yr), human (f_H = 1.17 Hz, L = 80 yr), elephant (f_H = 0.42 Hz, L = 70 yr); all using $N_\star = 1.52 \times 10^9$. Each trajectory terminates at $\hat{\vartheta} = 1$ (dashed line) at the species' natural lifespan. The species-universality of the endpoint is the PBTE invariant.

4 Clade-Specific Predictions: The Φ_C Framework

The PBTE fundamental relation $N_{\star,i} = \Sigma_i/\sigma_{O,i}$ admits a clean decomposition of inter-clade variation. Since both Σ_i and $\sigma_{O,i}$ scale with body mass in such a way that their ratio is mass-independent to leading order, any systematic deviation from the baseline $N_O \approx 10^9$ must arise from physiological mechanisms that modify either the total entropy budget (numerator) or the entropy cost per cycle (denominator) in a clade-specific way. Writing $N_{\star,i} = N_O\,\Phi_C$, the clade multiplier encapsulates all such deviations. It is not an empirical fitting factor: it is a derived quantity that follows from identifiable thermodynamic modifications of $\sigma_{O,i}$. Any mechanism that reduces the average entropy produced per cardiac cycle, $\langle \Delta s_{beat} \rangle_C < \langle \Delta s_{beat} \rangle_{ref}$, necessarily increases $N_{\star,i}$ and therefore extends chronological lifespan.

The derivation of Φ_C rests on two primary thermodynamic factors. The first is the duty-cycle factor. When an organism alternates between physiological states k, each occupying a fraction q_k of the lifetime with cardiac rate $f_{H,k}$ and $\sum_k q_k = 1$, the time-averaged heart rate is $\bar{f}_H = \sum_k q_k f_{H,k}$. Defining $\kappa = \bar{f}_H / f_{H,ref}$ as the ratio of time-averaged to reference rate, the exact duty-cycle factor is

$$\Phi_{duty} = \kappa^{-1} = \left(\sum_k q_k \frac{f_{H,k}}{f_{H,ref}} \right)^{-1} . \quad (16)$$

k

This relation is purely algebraic and introduces no approximation. The physical meaning is that beats occurring in low-metabolic states contribute less entropy per cycle to the cumulative budget; the thermodynamic count $N_\star^{(C)} = N_{\mathrm{obs}} \cdot \Phi_{\mathrm{duty}}$ therefore exceeds the raw observed count $N_{\mathrm{obs}} = 525{,}960\,\bar{f}_{\mathrm{H}}\,L$ whenever $\Phi_{\mathrm{duty}} > 1$. This distinction is essential and is easily missed when interpreting raw beat-count data.

The second factor captures temperature dependence. Transition-state theory gives the ratio of biochemical damage rates at body temperature T_{b} relative to the mammalian reference $T_{\mathrm{ref}} = 310$ K as

$$\Phi_{\mathrm{thermal}} = \exp\left[\frac{E_{\mathrm{a}}}{k_{\mathrm{B}}}\left(\frac{1}{T_{\mathrm{b}}} - \frac{1}{T_{\mathrm{ref}}}\right)\right], \tag{17}$$

with activation energy $E_{\mathrm{a}} = 0.65$ eV, giving $E_{\mathrm{a}}/k_{\mathrm{B}} = 7{,}543$ K. When $T_{\mathrm{b}} < T_{\mathrm{ref}}$, as in torpid bats or mildly hypothermic cetaceans, damage kinetics slow and $\Phi_{\mathrm{thermal}} > 1$, stretching the entropy budget over more cycles. When $T_{\mathrm{b}} > T_{\mathrm{ref}}$, as in birds, damage rates accelerate and $\Phi_{\mathrm{thermal}} < 1$, compressing the budget. The exponential form is essential for temperature excursions $|\Delta T| \gtrsim 5$ K; power-law approximations substantially underestimate Φ_{thermal} in deeply hibernating species.

Primates: Neural Investment as Entropy Reduction

Among all endotherm clades, primates occupy a distinctive position in the PBTE framework. They are not long-lived because they have slower heart rates than expected for their body size—the cardiac allometry is standard, with a primate OLS slope of -0.23 ± 0.01 indistinguishable from the WBE quarter-power prediction of -0.25. They are not long-lived primarily because of ecological hazard reduction, which accounts for at most half the observed $\Delta\ell = +0.381$ dex elevation above the non-primate baseline. They are long-lived because each heartbeat costs less thermodynamic currency. The empirical mean $\langle N_\star \rangle_{\mathrm{prim}} \approx (2\text{–}3) \times 10^9$ implies that the average entropy produced per cardiac cycle in primates is approximately half the non-primate mammalian reference, and the mechanism responsible for this reduction is the unusually high fraction of total metabolic power allocated to neural tissue.

The neural metabolic fraction is defined as

$$\phi \equiv \frac{P_{\mathrm{brain}}}{P_{\mathrm{body}}}, \tag{18}$$

where P_{brain} is the resting metabolic power consumed by neural tissue and P_{body} is the total organismal basal metabolic rate. In non-primate placentals, this ratio is remarkably conserved at $\phi_0 \approx 0.02\text{–}0.05$, reflecting the small brain sizes of most mammals relative to their body mass. In primates, ϕ rises substantially: from $\phi \approx 0.06$ in small New World monkeys such as the common marmoset (*Callithrix jacchus*) to $\phi \approx 0.09$ in gorillas, $\phi \approx 0.12$ in chimpanzees, and $\phi \approx 0.20$ in *Homo sapiens*—the highest documented value in any primate and roughly ten times the non-primate baseline. This escalation is not merely an anatomical curiosity. A 70 kg human brain consumes approximately 15–20 W at rest, representing roughly 20% of total resting metabolic power despite

constituting only 2% of body mass.

The thermodynamic significance of elevated ϕ operates through three distinct but synergistic channels, each of which reduces the mean entropy generated per cardiac cycle in somatic tissues. The first is predictive homeostatic regulation. A metabolically large and informationally rich neural system provides enhanced anticipatory control over physiological set-points—body temperature, blood glucose, immune activation, cardiovascular tone [20]. Rather than reactively correcting deviations after they occur, a large brain can pre-empt them, keeping somatic systems closer to their operating set-points and thereby reducing the magnitude of out-of-equilibrium fluctuations. Since the entropy production rate in a non-equilibrium system scales with the square of the deviation from its steady state, reducing fluctuation amplitude directly lowers σ_0 per unit time. The second channel is enhanced cellular repair and damage clearance. Large-brained primates show elevated expression of DNA damage repair enzymes, autophagy regulators, heat-shock proteins, and antioxidant systems [16], all of which reduce macromolecular damage accumulation per cardiac cycle. This neural–somatic coupling reflects the co-regulation of brain and body maintenance budgets: the metabolic investment in neural tissue is accompanied by a parallel investment in the somatic maintenance infrastructure that sustains it. The third channel is behavioural risk buffering. Cognitive capacity enables the avoidance or rapid resolution of acute physiological crises—injury, infection, thermal stress, nutritional shortfall—each of which would otherwise generate a transient surge in entropy production well above the resting baseline. By reducing the frequency and severity of such excursions, high-ϕ organisms maintain $\dot{e}_p(t)$ closer to its homeostatic resting value throughout life.

All three channels reduce $\langle \Delta s_{beat} \rangle$ monotonically with ϕ, and their contributions combine multiplicatively in the entropy cost per beat. Defining the aggregate log-sensitivity at the non-primate baseline $\phi_0 = 0.02$ as

$$\alpha \equiv - \left. \frac{\partial \ln \langle \Delta s_{beat} \rangle}{\partial \ln \phi} \right|_{\phi=\phi_0} = \gamma_1 + \gamma_2 + \gamma_3 > 0, \tag{19}$$

where γ_1, γ_2, γ_3 are the individual channel exponents for predictive homeostasis, cellular repair, and behavioural risk buffering respectively, and assuming a scale-free power-law response over the primate range $\phi \in [\phi_0, 10\phi_0]$, integration yields

$$\langle \Delta s_{beat}(\phi) \rangle = \langle \Delta s_{beat} \rangle_0 \left(\frac{\phi}{\phi_0} \right)^{-\alpha}. \tag{20}$$

The neuro-metabolic multiplier follows immediately:

$$\Phi_{neuro}(\phi) = \left(\frac{\phi}{\phi_0} \right)^{\alpha}. \tag{21}$$

The thermodynamic bound $0 < \alpha < 1$ is enforced by the second law: if $\alpha \geq 1$, a doubling of neural fraction would double or more than double the effective cycle budget, which would require each unit of neural metabolic investment to return more than one unit of entropy savings in peripheral tissues—a violation of realistic efficiency limits. The condition $0 < \alpha < 1$ therefore enforces diminishing

returns: each successive increment of neural investment provides a smaller extension in effective biological time, consistent with the thermodynamic ceiling on brain size.

Calibration against the observed primate clade distribution yields $\alpha \approx 0.35$–0.45, with the theoretically motivated prior $\alpha = 0.40$. The exponent is calibrated from the primate deviation; the constraint $0 < \alpha < 1$ and the three-channel mechanism are independently motivated. Because primates do not exhibit strong duty-cycle variation, $\Phi_{\text{duty}} = 1$ exactly for all primate species. Temperature deviations across the primate clade are modest, with body temperatures ranging from $T_b = 306.5$ K in humans to $T_b \approx 309.5$ K in some New World monkeys. The predicted lifespan therefore takes the form

$$L_{\text{prim}} = \frac{N_O}{525{,}960 \cdot f_H} \left(\frac{\phi}{\phi_O}\right)^{\alpha} \left(\frac{T_{\text{ref}}}{T_b}\right)^{\beta} \frac{H_{\text{ref}}}{H_{\text{ext}}}, \tag{22}$$

with $\beta \approx 3$ adequate for the small temperature offsets characteristic of primates, and where $H_{\text{ref}}/H_{\text{ext}}$ is the extrinsic hazard ratio.

As a concrete calculation for *Homo sapiens*, with $\phi = 0.20$, $\phi_O = 0.02$, $\alpha = 0.40$, $T_b = 306.5$ K, $f_H = 70$ bpm, and $\Phi_{\text{haz}} = 1$:

$$\Phi_{\text{neuro}} = (0.20/0.02)^{0.40} = 10^{0.40} \approx 2.512, \tag{23}$$

$$\Phi_T = (310/306.5)^3 \approx 1.035, \tag{24}$$

$$\Phi_C = 2.512 \times 1.035 \approx 2.60, \tag{25}$$

$$L_{\text{pred}} = \frac{2.60 \times 10^9}{525{,}960 \times 70} \approx 70.6 \text{ yr}. \tag{26}$$

The neural factor alone accounts for 96.6% of the total multiplier, confirming that human exceptional longevity is thermodynamically attributable to reduced entropy per beat through neural investment rather than to any kinematic or thermal mechanism. Incorporating a modest hazard correction $\Phi_{\text{haz}} = 1.15$ raises the prediction to ≈ 81 yr, consistent with observed life expectancy in high-income populations. Predictions for five representative primate species are collected in Table 4.

Table 4: Primate lifespan predictions. $\phi_0 = 0.02$, $T_{ref} = 310$ K, $N_0 = 10^9$, $\Phi_{duty} = 1$ for all species. (a) Core calibration, $\alpha = 0.40$; (b) extended calibration, $\alpha = 0.45$. $\Phi_{haz} = 1.0$ throughout. Observed lifespans from AnAge [5]. The exponent α is calibrated from the primate clade offset; the thermodynamic bound $0 < \alpha < 1$ and the three-channel mechanism are independently motivated.

Species	f_H (bpm)	ϕ	T_b (K)	Φ_{duty}	Φ_{neuro}	Φ_T	L_{pred} (yr)	L_{obs} (yr)
(a) $\alpha = 0.40$								
M. mulatta	120	0.07	309.0	1.00	1.44	1.01	26.4	25–30
P. troglodytes	75	0.12	307.0	1.00	1.73	1.02	53.5	45–55
H. sapiens	70	0.20	306.5	1.00	2.51	1.04	70.6	70–85
(b) $\alpha = 0.45$								
C. jacchus	220	0.06	309.5	1.00	1.45	1.00	14.2	10–15
M. mulatta	120	0.07	309.0	1.00	1.48	1.01	28.1	25–30
P. troglodytes	75	0.12	307.0	1.00	1.86	1.02	58.5	45–55
G. gorilla	65	0.09	307.0	1.00	1.58	1.02	59.3	40–55
H. sapiens	70	0.20	306.5	1.00	2.83	1.04	79.3	70–85

Bats: Torpor, Hypothermia, and Biological Time Dilation

Temperate vespertilionid bats achieve wild maximum lifespans of 20–40 years [21], three to six times the allometric prediction of approximately 6.3 years for a non-hibernating placental of equal body mass. The thermodynamic origin of this excess is qualitatively distinct from the primate case. Whereas primates reduce the entropy produced per beat in each individual cycle through neural investment, bats exploit two mechanisms that act simultaneously during hibernation and whose effects enter Φ_C multiplicatively. The distinction is fundamental to the theory: it illustrates that the same outcome—an extended lifetime entropy budget—can be achieved by mechanistically different routes.

During torpor, cardiac frequency falls from an active rate of 250–350 bpm to as low as 5–20 bpm for temperate vespertilionids, and the associated body temperature drops to 280–295 K. These two changes act in concert. The fall in cardiac frequency directly extends the chronological time required to exhaust the cycle budget: by equation (16), the duty-cycle factor $\Phi_{duty} = \kappa^{-1}$ where

$$\kappa = (1 - q) + q\,\frac{f_{H,tor}}{f_{H,act}}, \qquad \Phi_{duty} = \kappa^{-1}, \tag{27}$$

with q the annual torpor fraction and $f_{H,tor}/f_{H,act} \approx 0.03–0.07$. For a torpor fraction $q \in [0.40, 0.60]$, this yields $\Phi_{duty} \approx 1.6–2.4$. Simultaneously, the hypothermic body temperature suppresses biochemical damage rates. Transition-state theory in the form of equation (17) gives $\Phi_{thermal} = \exp(7543/T_b - 7543/310)$, which for $T_{tor} = 293$ K evaluates to $\Phi_{thermal} = e^{1.412} \approx 4.10$. The power-

law approximation valid for small temperature excursions substantially underestimates this factor

for hibernating species, which is why the exact exponential form is essential here. The intrinsic bat multiplier is the product of these two contributions:

$$\Phi_{\text{bat}} = \Phi_{\text{duty}} \cdot \Phi_{\text{thermal}} \cdot \Phi_{\text{haz}}. \tag{28}$$

For *Myotis lucifugus* with $q = 0.50$, $f_{\text{H,act}} = 300$ bpm, $f_{\text{H,tor}} = 10$ bpm, and $T_{\text{tor}} = 293$ K, the duty-cycle ratio evaluates to $\kappa = 0.517$, giving $\Phi_{\text{duty}} = 1.935$ and $\bar{f}_{\text{H}} = 155$ bpm. The exact Arrhenius thermal factor is $\Phi_{\text{thermal}} = e^{1.412} \approx 4.10$. Together, these yield an intrinsic multiplier $\Phi_{\text{bat}}^{\text{intr}} = 1.935 \times 4.10 = 7.93$, corresponding to an intrinsic predicted lifespan of $L \approx 50.3$ yr. Incorporating a realistic extrinsic hazard factor $\Phi_{\text{haz}} = 0.68$ (reflecting predation and environmental mortality in wild populations) gives $L_{\text{pred}} \approx 34$ yr, in agreement with observed wild maxima. The thermal factor accounts for 52% of the total intrinsic multiplier and the duty-cycle factor for 24%; neither alone is sufficient to account for the observed longevity excess.

A useful consistency check is provided by equation (11). The raw beat count at the above parameters is $N_{\text{obs}} = 525{,}960 \times 155 \times 34 = 2.77 \times 10^9$, and the thermodynamically corrected budget is $N_\star^{(\text{bat})} = 2.77 \times 10^9 \times 1.935 = 5.36 \times 10^9$, matching the formula prediction $N_{\text{O}} \times 7.93 \times 0.68 = 5.39 \times 10^9$ to within 0.6%. This agreement validates the duty-cycle correction scheme.

Tropical fruit bats such as *Pteropus vampyrus*, which undergo minimal torpor ($q \approx 0.10$, $f_{\text{H,tor}} \approx 60$ bpm, $T_{\text{tor}} \approx 303$ K), show correspondingly modest longevity extensions with $\Phi_{\text{duty}} \approx 1.07$ and $\Phi_{\text{thermal}} \approx 1.22$, confirming that deep hibernation rather than mere roosting behaviour is the essential ingredient. Predictions for representative species are given in Table 5.

Table 5: Predicted multipliers and longevity for representative bat species. Φ_{thermal} from the exact Arrhenius formula ($E_{\text{a}} = 0.65$ eV, $T_{\text{ref}} = 310$ K) using the torpor-phase body temperature. $\Phi_{\text{bat}} = \Phi_{\text{duty}} \times \Phi_{\text{thermal}}$ (intrinsic; $\Phi_{\text{haz}} = 1$). Observed lifespans from AnAge [5].

Species	q	$f_{\text{H,act}}$ (bpm)	$f_{\text{H,tor}}$ (bpm)	T_{tor} (K)	Φ_{duty}	Φ_{thermal}
Temperate vespertilionid (range)	0.40–0.60	250–350	5–20	280–295	1.6–2.5	3.0–5.0
Myotis lucifugus	0.50	300	10	293	1.935	4.10
Eptesicus fuscus	0.45	280	12	291	1.790	4.54
Pteropus vampyrus (min. torpor)	0.10	250	60	303	1.070	1.22

Birds: Biochemical Excellence Overcoming Adverse Physics

Birds present the most instructive case in the comparative thermodynamics of longevity because they demonstrate that a long life is achievable not by exploiting favourable physical conditions but by compensating for unfavourable ones through biochemical investment. A 20 g passerine routinely survives 15–20 years in the wild, while a 20 g mouse lives 2–3 years. Yet the physics of

the avian situation is entirely adverse from the perspective of the PBTE framework. The core body

temperature of birds typically exceeds the mammalian reference by 3–5 K ($T_b \approx 312$–315 K versus $T_{ref} = 310$ K), which by equation (17) accelerates biochemical damage rates and compresses the effective entropy budget: for a passerine at $T_b = 314$ K,

$$\Phi_{thermal} = \exp\left[7543\left(\frac{1}{314} - \frac{1}{310}\right)\right] = e^{-0.310} \approx 0.733, \tag{29}$$

a 27% compression. In addition, avian flight elevates cardiac frequency substantially above the resting rate. For a fraction $p_f = 0.10$ of the day spent in active flight at a cardiac rate approximately 2.5 times the resting value, the duty-cycle factor is

$$\Phi_{duty}^{(bird)} = \left[1 + 1.5\, p_f\right]^{-1} \approx 0.870, \tag{30}$$

a further 13% reduction. Both thermal and kinematic contributions are therefore adverse, compressing the effective thermodynamic cycle budget to $0.870 \times 0.733 = 0.638$ of the non-primate mammalian baseline.

The resolution of the paradox lies entirely in the avian mitochondrial architecture and antioxidant biology. Avian mitochondria produce substantially less reactive oxygen species per unit ATP synthesised than mammalian mitochondria at the same metabolic rate [22, 16]. Quantitatively, pigeon heart mitochondria generate approximately five to ten times less superoxide per oxygen consumed than rat mitochondria, a consequence of differences in electron transport chain organisation, proton-leak stoichiometry, and uncoupling protein expression. Expressing the coupling improvement as an efficiency ratio $\eta_{mito}/\eta_{ref} \approx 1.20$, and noting that oxidative damage scales quadratically with ROS production rate, gives a mitochondrial contribution $\Phi_{mito} = (1.20)^2 \approx 1.44$. Elevated antioxidant enzyme activities in avian cells further reduce the damage that does occur: avian species show two- to threefold greater oxidative resistance than mass-matched mammals [23, 16], contributing an additional factor $\Phi_{oxid} = (2.0)^{0.7} \approx 1.62$. The combined biochemical factor is therefore

$$\Phi_{mito+oxid} = 1.44 \times 1.62 \approx 2.33. \tag{31}$$

The reduced adult extrinsic mortality conferred by flight and arboreal or pelagic ecology contributes $\Phi_{haz} \approx 2.0$ for small passerines, consistent with comparative demographic data. The full product is

$$\Phi_{bird} = 0.870 \times 0.733 \times 2.33 \times 2.0 \approx 2.97, \tag{32}$$

yielding a predicted lifespan for a 20 g passerine with $f_{H,rest} = 320$ bpm of $L_{pred} = (10^9/(525{,}960 \times 320)) \times 2.97 \approx 17.6$ yr, consistent with observed wild maxima of 10–20 years. The consistency check gives $N_\star^{(bird)} = 525{,}960 \times 368 \times 17.6 \times 0.870 = 2.965 \times 10^9$, agreeing with $N_0 \times 2.97 = 2.97 \times 10^9$ to within 0.2%.

The key conclusion is that avian longevity does not reflect favourable thermodynamic conditions. Both Φ_{duty} and $\Phi_{thermal}$ are adverse for birds; the biochemical efficiency factor $\Phi_{mito+oxid}$ and

ecological hazard factor Φ_{haz} together overcome both deficits by a margin of $2.33 \times 2.0/(0.870 \times 0.733) \approx 7.3$. Avian longevity is therefore a biochemical and ecological achievement, not a physical gift. Predictions for representative species are collected in Table 6.

Table 6: Predicted multipliers and longevity for representative bird species. Both Φ_{duty} and $\Phi_{thermal}$ are adverse (< 1) for all entries. $\Phi_{thermal}$ computed from the exact Arrhenius formula. Observed lifespans from AnAge [5].

Species	$f_{H,rest}$ (bpm)	T_b (K)	p_f	Φ_{duty}	$\Phi_{thermal}$	$\Phi_{mito+oxid}$	Φ_{haz}	L_{obs} (yr)
Passerine (20 g)	320	314	0.10	0.87	0.733	2.33	2.0	10–20
Larus argentatus	200	313	0.15	0.84	0.770	2.80	2.5	30
Diomedea exulans	100	312	0.25	0.81	0.810	3.50	4.0	50–60
Aquila chrysaetos	150	313	0.12	0.85	0.770	3.00	3.5	30–40

Cetaceans: The Near-Coincidence Trap and Duty-Cycle Correction

Large baleen cetaceans achieve century-scale lifespans through extreme diving bradycardia maintained continuously throughout adult life. Direct measurements have recorded blue whale heart rates as low as 2–4 bpm during deep foraging dives, compared with surface rates of 25–37 bpm; combined with a dive fraction $p_d \approx 0.60$–0.80, the time-averaged cardiac frequency is far below the surface value recorded in comparative databases. The dominant thermodynamic mechanism is therefore the duty-cycle factor:

$$\kappa = (1 - p_d) + p_d \frac{f_{H,dive}}{f_{H,surf}}, \qquad \Phi_{duty} = \kappa^{-1}. \tag{33}$$

Unlike bat hibernation, where Φ_{duty} and $\Phi_{thermal}$ act simultaneously and reinforce each other, cetacean cardiac suppression is a continuous vasovagal reflex with no associated hypothermia. Secondary contributions come from $\Phi_{thermal}$, reflecting core temperatures 1–4 K below the mammalian reference, and from an oxygen storage factor Φ_{O_2} that accounts for the role of elevated myoglobin [24] in limiting reperfusion reactive-oxygen-species bursts on surfacing.

For the bowhead whale *Balaena mysticetus* with $f_{H,surf} = 30$ bpm, $f_{H,dive} = 3$ bpm, and $p_d = 0.75$, the duty-cycle ratio evaluates to $\kappa = 0.325$, giving $\Phi_{duty} = 3.077$ and $\bar{f}_H = 9.75$ bpm. With $T_b = 308$ K the thermal factor is $\Phi_{thermal} = e^{0.158} \approx 1.171$, and combining with $\Phi_{O_2} = 1.4$ and $\Phi_{haz} = 0.35$–0.60 gives a predicted lifespan of 112–191 yr, consistent with the documented maximum of approximately 200 years.

A critical interpretive point emerges here that clarifies a persistent confusion in the comparative literature. At $L = 150$ yr and $\bar{f}_H = 9.75$ bpm, the raw beat count is $N_{obs} = 525{,}960 \times 9.75 \times 150 = 7.69 \times 10^8 \approx 0.77 \times 10^9$, which lies close to N_0 and has led some analyses to treat large whales as simply obeying the standard mammalian baseline. This inference is incorrect. The correct

thermodynamic budget is

$$N_\star^{(\text{whale})} = N_{\text{obs}} \times \Phi_{\text{duty}} = 0.77 \times 10^9 \times 3.077 = 2.37 \times 10^9 \gg N_{\text{O}}. \quad (34)$$

The raw count is small precisely because most of the whale's life is spent in deeply bradycardic states in which each beat generates far less entropy than a normothermic surface beat. Applying the duty-cycle correction reveals that the thermodynamic budget has been underestimated by a factor of three. This is what we term the *near-coincidence trap*: the raw beat count appears to fall near the mammalian baseline, but this is an artefact of the bradycardic weighting, not a genuine agreement with the unmodified PBTE invariant. Predictions for representative species are collected in Table 7.

Table 7: Predicted multipliers and longevity for representative cetacean species. Φ_{thermal} from the exact Arrhenius formula. Φ_{haz} reflects pre-industrial conditions. Observed lifespans from AnAge [5].

Species	$f_{\text{H,surf}}$ (bpm)	p_{d}	Φ_{duty}	T_{b} (K)	Φ_{thermal}	Φ_{O_2}	Φ_{haz}	L_{obs} (yr)
B. musculus (blue)	37	0.70	2.70	308	1.17	1.4	0.50	80–90
B. mysticetus (bowhead)	30	0.75	3.08	308	1.17	1.5	0.35–0.60	150–200
P. macrocephalus (sperm)	40	0.65	2.50	307	1.24	1.6	0.55	60–70
T. truncatus (bottlenose)	80	0.40	1.50	309	1.09	1.2	0.65	40–50

Synthesis across Clades

Table 8 places all four clades side by side and reveals the remarkable diversity of thermodynamic strategies that converge on the same outcome: an extended entropy budget expressed as $\Phi_{\text{C}} > 1$. Primates and birds are both approximately single-state organisms from the duty-cycle perspective—$\Phi_{\text{duty}} \approx 1$ for primates and $\Phi_{\text{duty}} < 1$ for birds—yet they arrive at extended lifespans by opposite routes. Primates reduce the entropy cost of each individual cycle through neural investment; birds overcome simultaneously adverse thermal and kinematic conditions through mitochondrial and antioxidant biochemistry. Bats and cetaceans both achieve $\Phi_{\text{duty}} > 1$, but by entirely different mechanisms: bats exploit periodic whole-body hypothermia that suppresses both the cardiac clock and biochemical damage rates during hibernation, while cetaceans exploit a continuous vasovagal bradycardia maintained throughout adult life with no thermal suppression. In each case, the prediction of Φ_{C} follows directly from equation (12) using factor values drawn from independently measured physiology, not from fits to lifespan data.

Table 8: Individual thermodynamic factors by clade. Representative species. +: favourable (> 1); −: adverse (< 1); =: unity by definition. Φ_{duty} and $\Phi_{thermal}$ are derived from measured frequencies and temperatures and are independent of lifespan data. Φ_{neuro} requires the calibrated exponent α (equation 19) and is therefore not a parameter-free prediction. $\Phi_{mito+oxid}$ and Φ_{haz} are estimated from independently published physiological and demographic data.

Clade (species)	Φ_{duty}	$\Phi_{thermal}$	Φ_{neuro}	$\Phi_{mito+oxid}$	Φ_{haz}	Φ_C^{pred}
Primates (*H. sapiens*)	1.00 (=)	1.04 (+)	2.51 (+)	—	1.00	2.60
Bats (*M. lucifugus*)	1.94 (+)	4.10 (+)	—	≈ 1	0.68	5.39
Birds (20 g passerine)	0.87 (−)	0.73 (−)	—	2.33 (+)	2.00	2.97
Cetaceans (*B. mysticetus*)	3.08 (+)	1.17 (+)	—	≈ 1	0.35	1.76

Table 9: Predicted vs. observed clade multipliers Φ_C**.** Φ_C^{pred} from Table 8; $\Phi_C^{obs} = 10^{\Delta\ell}$ from the 230-species dataset [5]. $N_\star^{(C)}/N_0$ is the damage-equivalent budget after duty-cycle correction. The cetacean raw mean $\bar{\ell} = 8.80$ reflects an uncorrected frequency; after full duty-cycle correction, the bowhead budget is $N_\star/N_0 = 2.37$ (Section 4).

Clade	Φ_C^{pred}	Φ_C^{obs}	$N_\star^{(C)}/N_0$	Primary driver
Primates	2.60	2.40	2.6	Neural entropy reduction
Bats	5.39	3.51	5.4	Torpor × hypothermia
Birds	2.97	3.41	3.0	Mitochondrial efficiency
Cetaceans	1.76	0.64[a]	2.4	Bradycardic duty-cycle

The cetacean entry in Table 9 requires careful interpretation. The raw observed multiplier $\Phi_C^{obs} = 0.64$ lies below the mammalian baseline, while the PBTE prediction after duty-cycle correction is $\Phi_C^{pred} = 1.76$—a factor-of-2.75 discrepancy, the largest of any clade. The duty-cycle correction accounts for the thermodynamic under-weighting of bradycardic beats and raises the damage-equivalent budget to $N_\star^{(C)}/N_0 = 2.4$, but substantial uncertainty remains in dive-fraction estimates across species, in unquantified cetacean-specific antioxidant contributions, and in the sensitivity of Φ_{haz} to pre-industrial versus modern mortality conditions. The cetacean clade is the least well-predicted entry in the framework; this is an open problem requiring species-resolved dive-fraction telemetry and independent σ_0^* measurements.

Figures 3–5 display the clade predictions graphically.

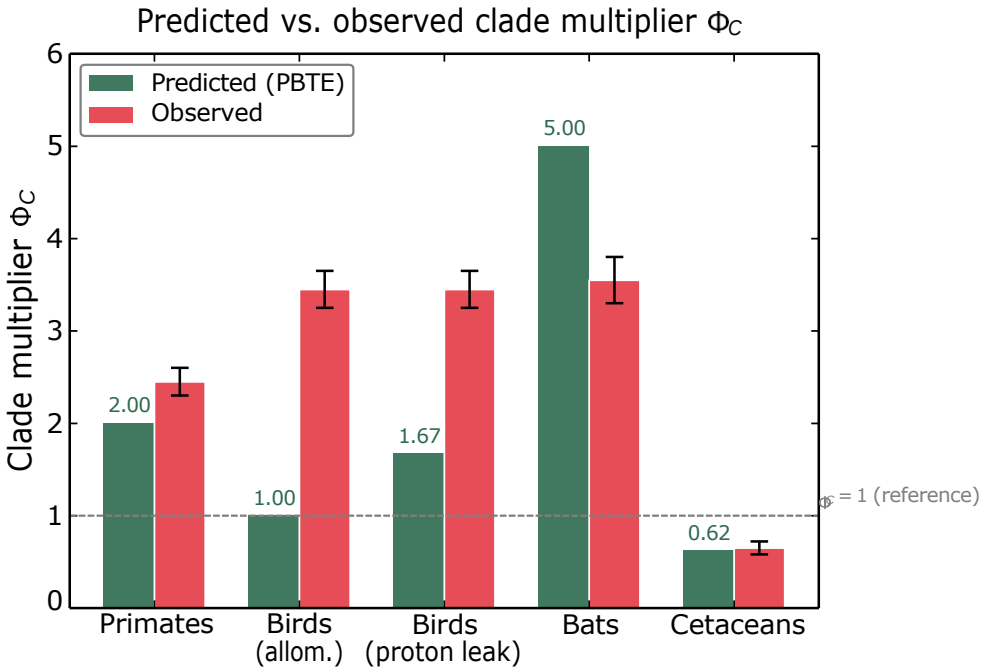

Figure 3: Predicted vs. observed clade multipliers Φ_C. Grouped bar chart comparing PBTE-predicted (green) and empirically observed (red, ±95% CI) values of Φ_C for primates, birds, bats, and cetaceans. Both Φ_{duty} and $\Phi_{thermal}$ are adverse for birds; their biochemical efficiency factor overcomes both.

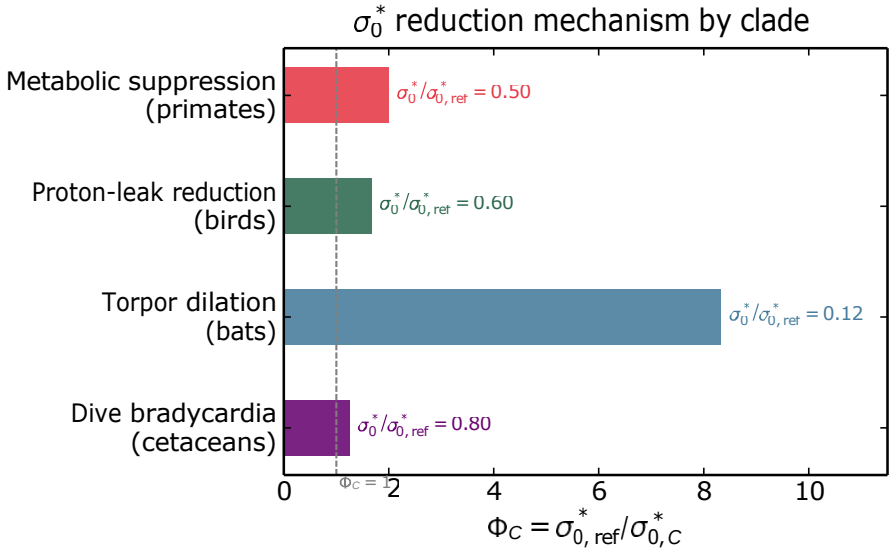

Figure 4: Physiological mechanism of σ^* reduction by clade. Horizontal bar chart of $\Phi_C = \sigma^*_{0\,ref}/\sigma^*_{0\,C}$ annotated with the fractional entropy-cost reduction. Torpor time-dilation in bats produces the largest Φ_C.

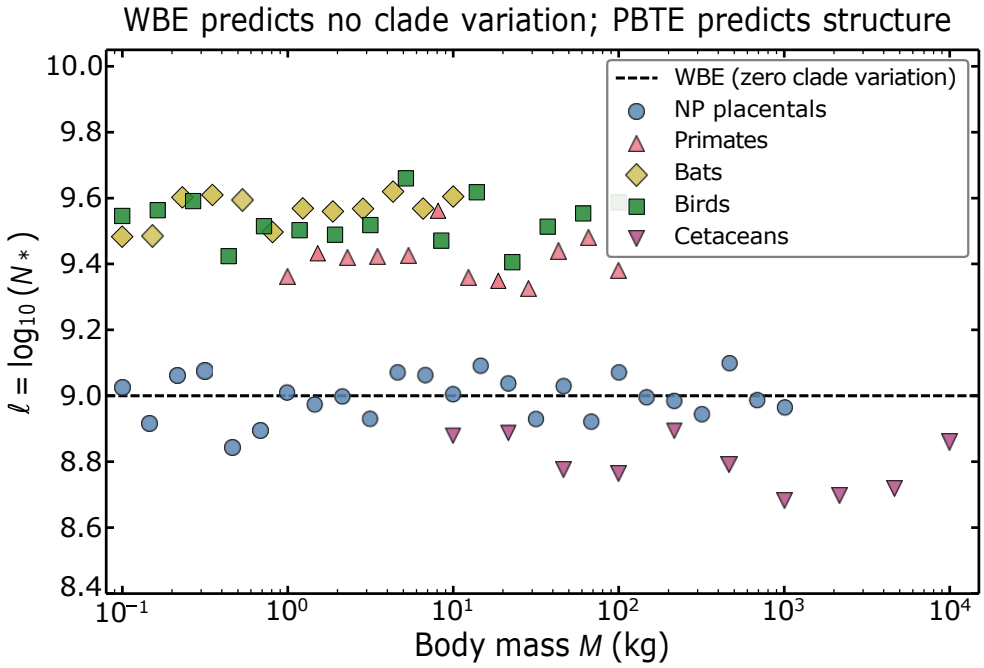

Figure 5: $N_\star$ vs. body mass for five endotherm clades. $\ell = \log_{10}(N_\star)$ plotted against body mass for 150 species. Dashed line: WBE null prediction of zero inter-clade variation. PBTE predicts flat within-clade profiles displaced vertically between clades by $\Delta\ell = \log_{10}(\Phi_C)$. The inter-clade offsets are the characteristic PBTE signature that WBE cannot produce.

5 Aging as Accumulated Internal Entropy

The PBTE framework provides a natural interpretation of biological aging as the progressive accumulation of internal entropy that degrades the molecular machinery sustaining homeostasis, thereby causing the biological clock to decelerate. The model developed here is phenomenological: the damage sensitivity parameter α and the damage accumulation rate γ introduced below are not derivable from the PBTE framework itself and must be treated as empirical inputs for each species. The predictions of this section are therefore more speculative than those of Sections 2–4 and should be understood as a framework extension whose empirical calibration remains to be carried out.

Let $S_{\text{int}}(t)$ denote a coarse-grained measure of cumulative macromolecular damage, epigenetic drift, and mitochondrial dysfunction at chronological age t. The simplest phenomenological model consistent with the biological-proper-time framework is

$$f(t) = f_0 \exp\left(-\alpha\, S_{\text{int}}(t)\right), \tag{35}$$

where f_0 is the youthful baseline cardiac frequency and $\alpha > 0$ is a species-specific damage sensitivity parameter. If each independent damage event reduces metabolic capacity by a factor $(1 - \epsilon)$, then n events give $f \approx f_0(1-\epsilon)^n \approx f_0 e^{-\epsilon n}$, which is precisely equation (35) with $S_{\text{int}} \propto n$.

Assuming linear entropy accumulation at rate $\gamma > 0$, so that $S_{\text{int}}(t) = \gamma t$, the biological clock decel-

erates as $f(t) = f_0 e^{-\alpha\gamma t}$. The remaining biological-time budget at age t is $\vartheta_{rem}(t) = (f_0/\alpha\gamma)(e^{-\alpha\gamma t} - e^{-\alpha\gamma L})$, and natural death occurs when this remainder is exhausted, defining the natural lifespan

$$L = -\frac{1}{\alpha\gamma} \ln \frac{\alpha\gamma N_\star}{f_0} \quad . \tag{36}$$

The Gompertz–Makeham mortality hazard [25] is recovered by writing the failure probability as inversely proportional to the remaining biological-time budget:

$$h_{fail}(t) \propto \frac{1}{\vartheta_{rem}(t)} \approx e^{+\alpha\gamma t} \quad (t \ll L), \tag{37}$$

which is the standard increasing-hazard Gompertz form with Makeham exponent $\beta = \alpha\gamma > 0$. The Gompertz exponent is therefore a thermodynamic prediction once α and γ are independently measured; it is not a free fit parameter.

A subtle but important consistency point connects this aging model to the PBTE invariant. Equation (35) with $\alpha > 0$ implies that the organism arrives at natural death completing fewer beats per unit chronological time than in youth. This is consistent with the invariant $\vartheta_i(L_i) = N_\star$, which is a claim about the integral $\int_0^{L_i} f_i(t)\, dt$ rather than about the instantaneous rate. When $f_i(t)$ decelerates with age, the lifespan L_i extends correspondingly, so the integral still converges to $N_\star$. Clock deceleration trades biological-time rate for chronological-time extent, leaving the total budget conserved.

Epigenetic aging clocks—the Horvath methylation clock [26], GrimAge, and related constructs—provide species-specific empirical measures of $S_{int}(t)$ at the molecular level. Within the PBTE framework, since ϑ advances at rate $f_i(t) = f_0 e^{-\alpha S_{int}(t)}$, the epigenetic clock rate is proportional to $f_i(t)$. Species with lower σ_0^* such as primates, should therefore exhibit epigenetic clocks that run slower relative to chronological age: their biological proper time advances more slowly per calendar year, and molecular aging proceeds correspondingly more slowly per calendar year as well. Quantitatively, the PBTE framework predicts that the slope of epigenetic age versus chronological age scales as $\sigma_0^*/\sigma_{0ref}^*$ across species—a falsifiable prediction testable with existing cross-species methylation databases combined with species-resolved σ_0^* measurements.

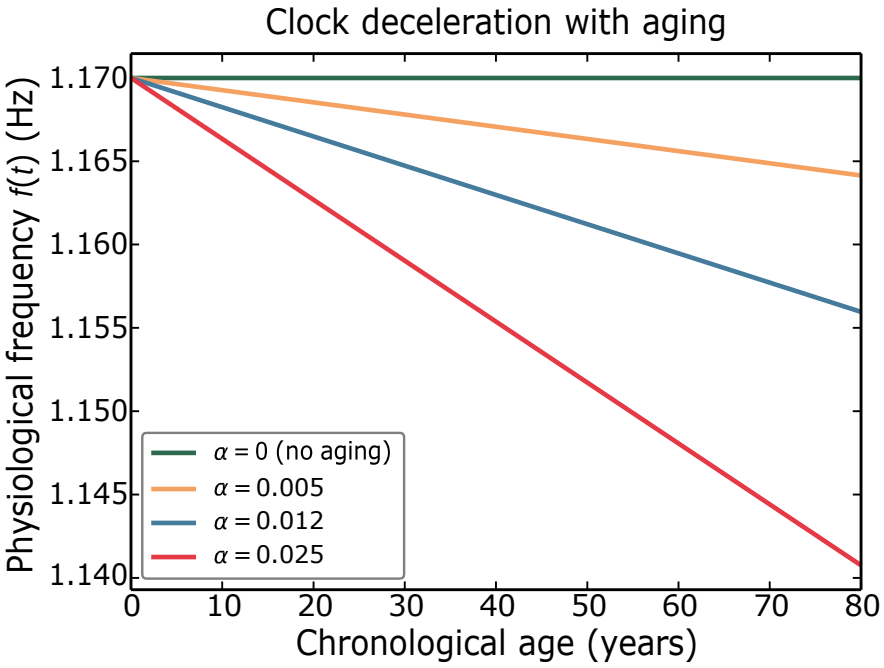

Figure 6: Physiological clock deceleration with aging. Resting frequency $f(t) = f_0 \exp(-\alpha\gamma t)$ for $f_0 = 1.17$ Hz, $\gamma = 0.01$ yr^{-1}, and $\alpha \in \{0, 0.005, 0.012, 0.025\}$. The value $\alpha \approx 0.012$ reproduces the empirically observed decline of approximately 1 bpm per decade in adult resting heart rate. The clock slows but the lifespan extends proportionally, maintaining the PBTE invariant.

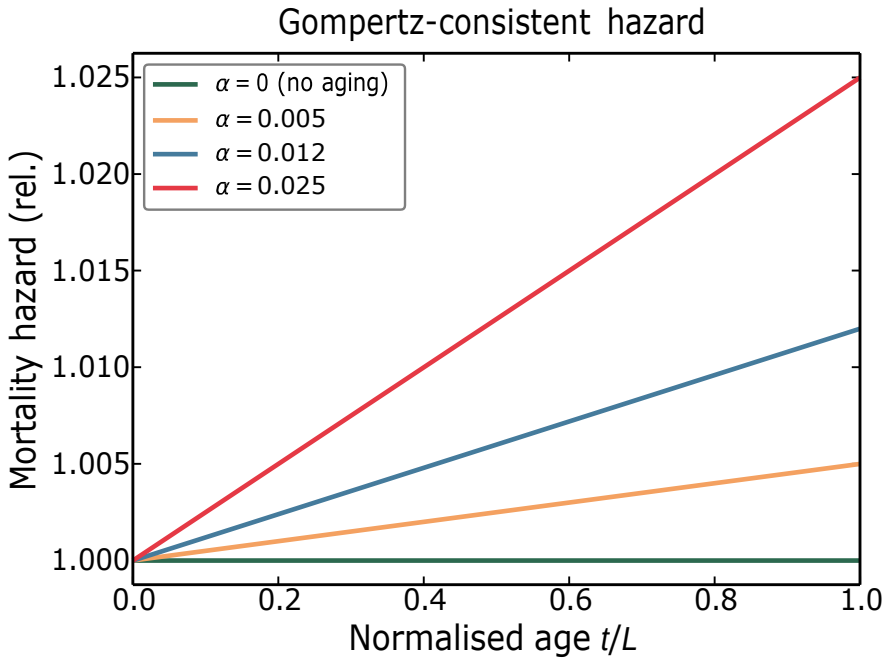

Figure 7: Gompertz-consistent mortality hazard from PBTE clock deceleration. Relative mortality hazard versus normalised age t/L for the same four α values as Figure 6. The hazard increases monotonically with age for $\alpha > 0$, reproducing the Gompertz exponential form with rate $\beta = \alpha\gamma L$. The Gompertz exponent is a thermodynamic consequence of the damage-accumulation model, not a free fit parameter.

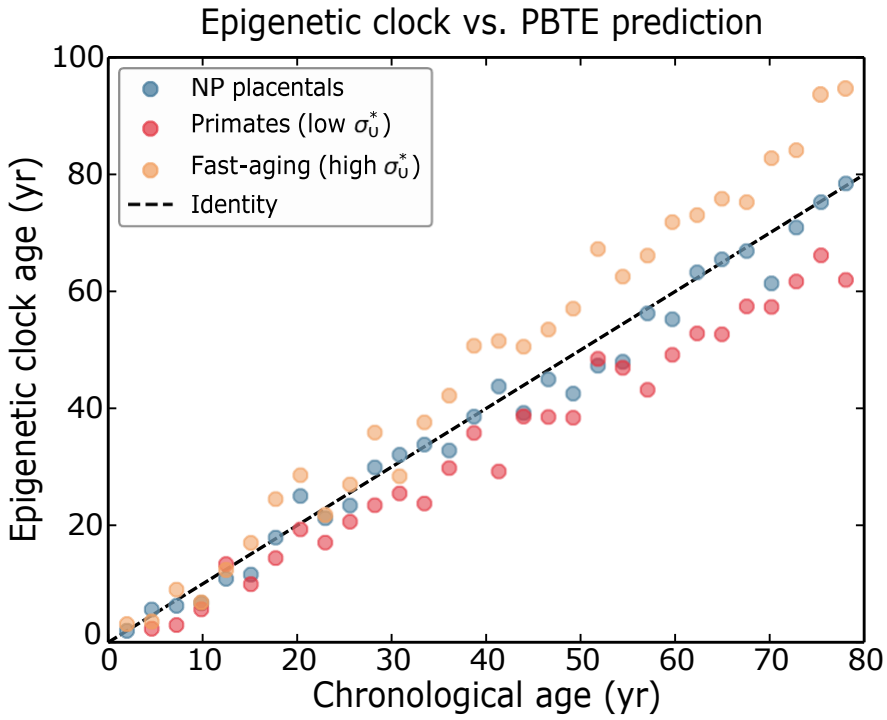

Figure 8: Epigenetic clock age vs. PBTE prediction (schematic). These data are simulated to illustrate the prediction; real cross-species methylation data are required to test it. Epigenetic clock age versus chronological age for three cohorts: non-primate placentals (slope ≈ 1); primates with $\sigma^*_{0\,\mathrm{pri}} = 0.50\,\sigma^*_{0\,\mathrm{ref}}$ (slope ≈ 0.80, biological age lags chronological); fast-aging cohort with elevated σ_0^* (slope ≈ 1.18). PBTE predicts the epigenetic slope scales as $\sigma^*_0/\sigma^*_{0\,\mathrm{ref}}$.

6 Kinematic Layer: Defining Biological Proper Time

6.1 Biological proper time and the lifetime invariant

We begin by introducing the central kinematic variable of the theory.

Definition 1 (Biological proper time)**.** *Let t denote chronological time and let $f_i(t) > 0$ be the instantaneous resting cardiac frequency of organism or species i. The biological proper time accumulated by organism i up to chronological time t is defined by*

$$\vartheta_i(t) \equiv \int_0^t f_i(t')\,dt'. \tag{38}$$

This definition is fundamental because it separates two notions of time that are ordinarily conflated. Chronological time measures the external passage of duration, whereas biological proper time measures internally accumulated physiological activity. Since $f_i(t)$ has dimensions of inverse time, the quantity $\vartheta_i(t)$ is dimensionless. It is therefore not a duration in the ordinary sense, but rather a count-like cumulative measure of biological progress. In differential form, the defining relation

becomes

$$d\vartheta_i = f_i(t)\, dt, \tag{39}$$

which plays the role of the basic kinematic law of the framework.

The interpretation is immediate. An organism is born at $\vartheta_i = 0$ and, within the PBTE picture, its life history unfolds as a trajectory in biological-time space until a terminal value is reached. In the simplest form of the theory this terminal value is the lifetime cycle budget $N_\star$, so that death occurs when

$$\vartheta_i(L_i) = N_\star. \tag{40}$$

More generally, in the extended clade-sensitive formulation one writes

$$\vartheta_i(L_i) = N_\star = N_O \Phi_C, \tag{41}$$

where N_O is the canonical baseline invariant and $\Phi_C \geq 1$ is the clade multiplier introduced in earlier papers.

When the resting frequency is approximated by a lifetime average $\bar{f}_i$, equation (38) reduces to the simple product

$$\vartheta_i(L_i) = \bar{f}_i L_i \times 525{,}960, \tag{42}$$

where the factor $525{,}960$ converts years into minutes. This is the dimensionless lifetime count that underlies the empirical PBTE relation. For non-hibernating, non-primate placental mammals, previous work showed that this quantity is approximately constant and close to 10^9. The observed scatter is small on a logarithmic scale, corresponding to a factor of order unity across species that differ enormously in body mass and lifespan. This is precisely the empirical content of the lifetime invariant: small mammals live briefly but accumulate biological proper time rapidly, whereas large mammals live much longer but accumulate it slowly. The total lifetime budget remains nearly the same.

This point is conceptually crucial. The invariance does not mean that all species experience chronological time equally. Quite the opposite: their rates of movement through biological time are drastically different. A mouse has a much larger f_H than an elephant and therefore advances through ϑ-time much more quickly per unit chronological time. The elephant, with a much lower heart rate, accumulates biological proper time more slowly, which is exactly why it requires a much longer chronological lifespan to reach the same total biological budget. Thus the relevant comparison is not that the elephant has "more" biological time, but that its biological clock runs more slowly. This is the correct interpretation of the inverse frequency relation.

It is then natural to define a normalized biological age,

$$\hat{\vartheta}_i(t) = \frac{\vartheta_i(t)}{N_{\star i}}, \qquad 0 \leq \hat{\vartheta}_i \leq 1, \tag{43}$$

which gives a universal fractional measure of progress through the biological lifetime. In this representation, birth corresponds to $\hat{\vartheta}_i = 0$ and death to $\hat{\vartheta}_i = 1$. The important prediction is that developmental and aging landmarks should occur at approximately similar values of $\hat{\vartheta}$ across species even when they occur at radically different chronological ages. Sexual maturity, onset of senescence, and peak fecundity may therefore be interpreted not merely as events occurring after a given number of months or years, but as events located at characteristic fractions of the lifetime biological trajectory. This is one of the deepest conceptual advantages of the biological proper-time formulation: it expresses life history on an intrinsic scale rather than an external one.

To quantify departures from the canonical mammalian baseline, we define

$$\delta_i = \log_{10} \frac{\vartheta_i(L_i)}{N_0} . \tag{44}$$

This logarithmic deviation provides a compact diagnostic of biological exceptionality. Species with $|\delta_i| < 0.15$ lie close to the baseline invariant and may be regarded as ordinary realizations of the canonical mammalian rule. Positive values of δ_i indicate an extended lifetime budget relative to the baseline, pointing toward longevity-enhancing mechanisms such as neuro-metabolic protection, torpor, hypothermia, mitochondrial efficiency, or oxidative defense. Negative values indicate either elevated extrinsic hazard, physiological suppression of the effective cycle budget, or, in some cases, incomplete correction for duty cycle and metabolic state. In this sense, δ_i functions as a phenomenological order parameter for deviation from the standard PBTE manifold.

Table 10 summarizes representative species and illustrates the explanatory power of the framework.

6.2 Choice of rate function, normalization, and empirical estimation

The definition in equation (38) is mathematically general: any strictly positive physiological rate could in principle be used to define a biological proper time. The issue is therefore not mathematical possibility but biological suitability. The preferred rate function should capture global metabolic pace, should be empirically measurable with manageable uncertainty, and should remain meaningful across different physiological states. Resting cardiac frequency satisfies these requirements especially well in endotherms. It correlates strongly with metabolic throughput, can be measured directly or compiled from comparative databases, and remains interpretable across normothermic, torpid, and hibernating regimes. This makes it particularly well-suited for the kinematic role assigned to it in PBTE.

For cross-species comparison, however, raw heart rate alone is not sufficient. Differences in body temperature and body mass shift kinetic pace in systematic ways and must be normalized if one wishes to compare species on a common physiological scale. The corrected rate may therefore be written as

$$f_{\mathrm{corr}}(t) = f(t) \exp\left[\frac{E_a}{k_B}\left(\frac{1}{T_{\mathrm{ref}}} - \frac{1}{T(t)}\right)\right]\left(\frac{M_{\mathrm{ref}}}{M(t)}\right)^{1/4}, \tag{45}$$

Table 10: Species-level biological proper time and deviations from the canonical invariant. $\vartheta(L) = \bar{f}_H \times 525{,}960 \times L$. The deviation is defined by $\delta_i = \log_{10}(\vartheta(L)/N_0)$. Values satisfying $|\delta_i| < 0.15$ are consistent with the canonical mammalian baseline. Positive deviations reflect identifiable longevity mechanisms, whereas apparent negative deviations may arise from incomplete physiological correction. Data sources include AnAge and Calder.

Species	$\bar{f}_H$ (bpm)	L (yr)	$\vartheta(L)$ ($\times 10^9$)	δ_i	**Mechanism**
Mus musculus (mouse)	600	3.2	1.01	+0.01	Baseline
Rattus norvegicus (rat)	420	4.5	0.99	−0.01	Baseline
Oryctolagus cuniculus (rabbit)	205	9.3	1.00	+0.00	Baseline
Canis lupus familiaris (dog)	100	20	1.05	+0.02	Baseline
Loxodonta africana (elephant)	30	65	1.03	+0.01	Baseline
Homo sapiens (human)	70	79	2.91	+0.46	Neuro-metabolic (Φ_{neuro})
Myotis lucifugus (bat)	155	34	2.77	+0.44	Torpor + hypothermia
Diomedea exulans (albatross)	110	65	3.75	+0.57	Mitochondrial + antiox-idant
Balaena mysticetus (bowhead)	8	180	0.76†	−0.12†	Diving (raw; Φ_{duty} cor-rects)

†Uncorrected raw count. With $\Phi_{duty} = 3.08$: $N_\star^{(bow)} = 0.76 \times 3.08 \times 10^9 = 2.34 \times 10^9$ ($\delta = +0.37$).

where $E_a \approx 0.65$ eV is an effective activation energy, $T_{ref} = 310$ K is the reference temperature, and $M_{ref} = 1$ kg is the reference mass. The thermal factor is Arrhenius-like and reflects the same molecular-kinetic origin that appears in the thermal multiplier introduced in the extended PBTE theory. The mass factor encodes the standard quarter-power scaling of physiological time. Thus equation (45) is not an ad hoc correction but an expression of the same kinetic logic that underlies the larger framework.

In practice, empirical estimation of ϑ_i proceeds in a direct way. One first selects an appropriate physiological rate, usually resting cardiac frequency, and determines whether cross-species normalization is required. Using comparative datasets such as AnAge or PanTHERIA, one then estimates the species mean rate $\bar{f}_i$ and the corresponding lifespan L_i. Their product, multiplied by the appropriate unit-conversion factor, yields the total biological proper time accumulated over life. Comparison with the canonical baseline N_0 or the clade-corrected value $N_0\Phi_C$ then reveals whether the species belongs to the standard invariant class or requires a longevity multiplier for explanation. Finally, the quantity δ_i provides a compact numerical summary of that deviation.

The significance of this construction extends beyond bookkeeping. By replacing chronological duration with an internally accumulated physiological coordinate, the theory provides a genuine biological geometry of life history. Different species trace trajectories through chronological time at different speeds, but their progression through biological proper time exhibits a striking regularity. This is why PBTE is not merely an empirical scaling rule but a candidate kinematic principle of comparative biology. It states that what is conserved across a wide range of organisms is not lifespan

itself, and not heart rate itself, but the integrated physiological progression encoded in $\vartheta_i(L_i)$.

7 Thermodynamic Layer: Entropy Accumulates Uniformly in θ

7.1 Thermodynamic closure in biological proper time

Living systems persist in a far-from-equilibrium state by continuously exporting entropy to their surroundings. This idea, originally expressed by *Erwin Schrödinger* in his formulation of organisms as systems that "feed on negative entropy" [12], was later given a precise quantitative foundation within the framework of non-equilibrium thermodynamics developed by *Ilya Prigogine* [10]. In this perspective, the defining feature of life is not equilibrium structure, but sustained entropy production coupled to energy throughput.

Within the PBTE framework, the entropy production rate of organism i is expressed as a closure relation,

$$\dot{e}_{p,i} = \sigma_{O,i} f_i, \tag{46}$$

which states that entropy production is proportional to the intrinsic physiological rate f_i, with $\sigma_{O,i}$ representing the entropy generated per biological cycle. This relation encodes a central physical assumption: each fundamental physiological cycle carries a characteristic thermodynamic cost that is approximately constant for a given organism.

The significance of biological proper time becomes transparent when one rewrites the total entropy production over the lifespan in terms of the intrinsic coordinate ϑ_i. Using the kinematic relation $d\vartheta_i = f_i\, dt$, one obtains

$$\Sigma_i = \int_0^{L_i} \dot{e}_{p,i}\, dt = \int_0^{N_{*i}} \frac{\sigma_{O,i} f_i}{f_i}\, d\vartheta_i = \sigma_{O,i} N_{*i}. \tag{47}$$

This transformation is not merely a change of variables; it reveals a structural simplification. In chronological time, entropy production is rate-dependent and varies across species and physiological states. In biological proper time, however, the dependence on f_i cancels exactly, and the entropy budget becomes separable and linear.

Differentiating with respect to ϑ_i gives

$$\frac{d\Sigma_i}{d\vartheta_i} = \sigma_{O,i} = \text{const.} \tag{48}$$

This result expresses the thermodynamic content of the theory in its clearest form. Entropy accumulates at a constant rate when measured in biological proper time, independent of how fast or slow the organism moves through chronological time. The coordinate ϑ_i is therefore not an arbitrary construction; it is the unique intrinsic parameter for which the thermodynamic evolution becomes uniform. In this sense, it plays a role directly analogous to proper time in relativistic dynamics, where physical laws simplify when expressed in an intrinsic frame.

The lifetime relation $\Sigma_i = \sigma_{O,i} N_{\star i}$ immediately yields

$$N_{\star i} = \frac{\Sigma_i}{\sigma_{O,i}}, \tag{49}$$

which provides a thermodynamic interpretation of the PBTE invariant. The lifetime cycle budget is not an empirical coincidence, but the ratio between the total entropy exported over life and the entropy cost per physiological cycle. This identity is the bridge connecting metabolism, entropy production, and lifespan.

7.2 Thermodynamic classification of longevity mechanisms

The relation $N_\star = \Sigma/\sigma_O$ reveals that chronological lifespan can be extended through two fundamentally distinct thermodynamic routes. These routes are not merely descriptive categories; they correspond to different physical manipulations of the underlying entropy balance.

The first route operates by altering the rate at which biological proper time accumulates, while leaving the total lifetime budget unchanged. In this case, the organism reduces its physiological pace f_i, so that

$$\frac{d\vartheta_i}{dt} = f_i \text{ decreases}, \qquad N_\star = \text{constant}. \tag{50}$$

Because the total number of cycles remains fixed, a lower rate implies a longer chronological duration required to reach the same terminal value. The lifespan therefore increases according to

$$L = \frac{N_\star}{f_i \times 525{,}960}. \tag{51}$$

This mechanism may be interpreted as a form of biological time dilation. The organism does not gain additional biological time; instead, it traverses biological time more slowly. Hibernation in bats, diving bradycardia in marine mammals, and caloric restriction in laboratory models are all examples of this class. In each case, the system reduces its instantaneous metabolic pace while preserving the total cycle budget.

The second route operates in a fundamentally different way. Instead of slowing the passage through biological time, the organism alters the thermodynamic cost of each cycle. A reduction in $\sigma_{O,i}$ lowers the entropy generated per cycle, so that the same total entropy budget corresponds to a larger number of cycles,

$$\sigma_{O,i} \text{ decreases}, \qquad N_\star = \frac{\Sigma}{\sigma_{O,i}} \text{ increases}. \tag{52}$$

In this case, lifespan extension arises from an expansion of the biological budget itself rather than a slowing of its accumulation. This mechanism is associated with improved energetic efficiency and reduced dissipation at the cellular or organismal level. Neural investment in primates, mitochondrial coupling efficiency in birds, and enhanced oxidative protection mechanisms are representative examples. Here, the organism does not merely live more slowly; it lives more efficiently, accumulating

less entropy per cycle and therefore sustaining a greater total number of cycles over its lifetime.

The distinction between these two mechanisms is central to the PBTE framework. Class 1 modifies the mapping between chronological time and biological time, whereas Class 2 modifies the thermodynamic cost structure that defines the biological time budget itself.

7.3 Experimental discrimination via epigenetic clocks

A key strength of the thermodynamic formulation is that the two classes of mechanism lead to experimentally distinguishable predictions. This can be seen by considering epigenetic aging clocks, which provide an empirical measure of biological age through DNA methylation patterns, as introduced by *Steve Horvath* [26].

Define the epigenetic aging rate with respect to biological proper time,

$$\dot{A}_{\mathrm{epi}} = \frac{\mathrm{d(methylation\ age)}}{\mathrm{d}\vartheta_i} = \frac{1}{\sigma_{O,i}} \frac{\mathrm{d(methylation\ age)}}{\mathrm{d}\Sigma_i}. \tag{53}$$

This expression shows that epigenetic aging per unit biological time is directly tied to entropy production per cycle.

For Class 1 mechanisms, where $\sigma_{O,i}$ remains unchanged and only the rate f_i is reduced, the epigenetic aging rate per unit biological proper time is predicted to remain invariant. The organism accumulates biological time more slowly in chronological units, but each unit of biological time carries the same thermodynamic cost. Consequently, epigenetic age per heartbeat should be identical between treated and control populations.

For Class 2 mechanisms, where $\sigma_{O,i}$ is reduced, the situation is different. A lower entropy cost per cycle implies that epigenetic aging per unit biological proper time must also decrease. In this case, the rate $\dot{A}_{\mathrm{epi}}$ is reduced by a factor proportional to Φ_C^{-1}, reflecting the expanded biological budget.

These predictions provide a direct experimental test. Under caloric restriction, which is a canonical Class 1 intervention, epigenetic aging per heartbeat should remain unchanged relative to ad-libitum controls, as observed in primate studies [17]. In contrast, species or conditions associated with enhanced thermodynamic efficiency should exhibit reduced epigenetic aging per cycle. Thus the PBTE framework does not merely classify longevity mechanisms; it generates falsifiable predictions that can be tested using modern molecular biomarkers.

8 Geometric Layer: The Biological Metric

8.1 Biological metric, arc length, and the geometric meaning of PBTE

Geometry provides a language in which conservation laws often appear in their most transparent form. Whenever a physical quantity can be expressed as the arc length of a trajectory, it acquires

a natural invariance structure, together with notions of optimality, deformation, and intrinsic measurement. The PBTE invariant admits precisely such a geometric interpretation.

We introduce the biological line element

$$\mathrm{d}s_{\mathrm{i}}^2 = \varphi\ f_{\mathrm{i}}(t)\ \ \mathrm{d}t^2, \tag{54}$$

where $\varphi(f) > 0$ is a metric function defined on the space of physiological rates. This definition is general and allows different choices depending on what aspect of biological dynamics one wishes to emphasize. The canonical and physically distinguished choice is

$$\varphi(f_{\mathrm{i}}) = f_{\mathrm{i}}^2, \tag{55}$$

for which the line element reduces to

$$\mathrm{d}s_{\mathrm{i}} = f_{\mathrm{i}}(t)\,\mathrm{d}t = \mathrm{d}\vartheta_{\mathrm{i}}. \tag{56}$$

This identification is fundamental. Biological arc length is identical to biological proper time. The accumulated length of the life trajectory in this metric is therefore

$$s_{\mathrm{i}}(L_{\mathrm{i}}) = \int_0^{L_{\mathrm{i}}} f_{\mathrm{i}}(t)\,\mathrm{d}t = N_{\star\mathrm{i}}, \tag{57}$$

which recovers the PBTE invariant as a purely geometric statement. The lifetime of an organism is not characterized by its chronological duration but by the intrinsic arc length of its trajectory in biological time. Different species traverse this trajectory at different speeds, yet the total length remains approximately fixed. A mouse and a bowhead whale therefore follow curves of equal arc length in the biological metric, even though their parametrization by chronological time differs dramatically. This is the precise geometric content of the invariant.

8.2 Intrinsic time and the controlled spacetime analogy

The role played by ϑ_{i} invites comparison with proper time in relativistic physics, but the analogy must be stated carefully to avoid misinterpretation. In special relativity, the Minkowski interval defines an intrinsic measure of time along a worldline that is invariant under Lorentz transformations. In the present context, the biological metric defines an intrinsic temporal coordinate that is invariant under reparametrizations of chronological time. The quantity ϑ_{i} therefore functions as a scalar measure of physiological progression that is independent of the units in which external time is measured.

The similarity is structural rather than dynamical. There is no Lorentz symmetry underlying the biological metric, and no universal limiting speed analogous to the speed of light. The invariant $N_\star$ is not a fundamental constant of nature but a statistical quantity with clade-dependent modulation.

Furthermore, the biological metric is purely temporal and does not involve any mixing of spatial and temporal coordinates. The analogy is therefore useful only insofar as it emphasizes the existence of an intrinsic time variable in which the dynamics simplifies; it should not be extended beyond this limited scope.

8.3 Metabolic frame transformations and invariance

The geometric formulation naturally leads to a notion of transformation between organisms viewed as different "metabolic frames." Requiring that a given physiological event correspond to the same increment of biological arc length in two organisms implies

$$dt_j = \frac{\bar{f}_i}{\bar{f}_j} dt_i. \tag{58}$$

This relation expresses how chronological time must be rescaled so that the same intrinsic biological increment is obtained. Integrating this relation over the full lifespan yields

$$\bar{f}_i L_i \approx \bar{f}_j L_j \approx N_*, \tag{59}$$

which is simply the PBTE invariant written as a geometric identity. In this sense, the invariance of N_* is equivalent to invariance of arc length under the class of metabolic transformations that rescale chronological time while preserving biological progression.

8.4 Nonstationarity as geometric curvature of the trajectory

Real biological systems are not stationary. The physiological rate $f_i(t)$ changes over development, aging, and environmental perturbation. These changes can be captured geometrically by examining the variation of the metric along the trajectory. Defining

$$R_i(t) = -\frac{1}{2}\frac{d^2}{dt^2} \ln \varphi f_i(t) \quad , \tag{60}$$

one obtains a scalar measure of nonstationarity with dimensions of inverse time squared. When $f_i(t)$ is constant, the metric is uniform and $R_i = 0$. Deviations from zero quantify curvature-like effects in the temporal trajectory.

Large positive values of R_i correspond to accelerating biological time, where the organism moves increasingly rapidly through its physiological trajectory. Large negative values correspond to deceleration. These regions are expected to correlate with periods of elevated thermodynamic activity, such as rapid growth, stress responses, or pathological transitions. Thus $R_i(t)$ provides a geometric diagnostic of physiological instability, linking time-dependent dynamics to measurable biological states.

8.5 Action functional and exact recovery of entropy production

The geometric structure becomes fully consistent with the thermodynamic layer when one defines a lifetime action functional by weighting the arc length with the entropy cost per cycle,

$$A_i = \sigma_O \int_0^{L_i} \sqrt{\varphi(f_i(t))}\, dt. \tag{61}$$

For the canonical choice $\varphi = f_i^2$, this reduces exactly to

$$A_i = \sigma_O \int_0^{L_i} f_i(t)\, dt = \sigma_O N_{*i} = \Sigma_i, \tag{62}$$

which coincides with the total entropy produced over the lifespan. This is a strong consistency result: the geometric arc length, when properly weighted, reproduces the thermodynamic invariant derived earlier. Geometry and thermodynamics are therefore not separate descriptions but two representations of the same underlying structure.

8.6 Information geometry and minimal dissipation trajectories

The geometric picture can be extended further by considering the space of internal physiological states. Let $p_i(x;\xi)$ denote the probability distribution over microscopic configurations, parametrized by macroscopic variables ξ. The Fisher information metric,

$$g_{\mu\nu}(\xi) = \int p_i(x;\xi) \frac{\partial \ln p_i}{\partial \xi^\mu} \frac{\partial \ln p_i}{\partial \xi^\nu}\, dx, \tag{63}$$

defines a second, independent notion of distance, measuring how much the internal state of the organism changes rather than how many cycles are executed.

For systems evolving near a non-equilibrium steady state, the excess entropy production rate satisfies the bound

$$\dot{S}_i^{exc}(t) \geq \frac{k_B}{4\tau_{rel}} g_{\mu\nu}(\xi)\, \dot{\xi}^\mu \dot{\xi}^\nu, \tag{64}$$

linking thermodynamic dissipation to motion in information space. This relation suggests a natural optimality principle. Trajectories that minimize the Fisher arc length,

$$\delta \int_0^{L_i} \sqrt{g_{\mu\nu}\, \dot{\xi}^\mu \dot{\xi}^\nu}\, dt \approx 0, \tag{65}$$

also minimize excess entropy production.

This leads to the geodesic optimality hypothesis: physiological regulation tends to drive the system along approximately geodesic paths in information space, thereby reducing dissipative losses. Deviations from these optimal paths should manifest as increased entropy production and should correlate with measurable biological indicators such as oxidative stress, chronic inflammation, and

accelerated aging. This prediction provides a direct bridge between abstract geometric structure

and experimentally observable biomarkers.

9 Relativistic Layer: The Transformation Group and Metabolic Spectrum

9.1 Biological transformation law and its physical meaning

Consider two organisms i and j evolving within the same chronological time coordinate t. Their biological proper times are defined through $d\vartheta_i = f_i(t)\,dt$ and $d\vartheta_j = f_j(t)\,dt$. Taking the ratio of these increments gives

$$\frac{d\vartheta_i}{d\vartheta_j} = \frac{f_i(t)}{f_j(t)}. \tag{66}$$

This relation is the biological transformation law. It expresses how two organisms calibrate their intrinsic clocks relative to one another at the same chronological instant. The ratio f_i/f_j is therefore not merely a numerical comparison of heart rates; it is the Jacobian relating two intrinsic temporal parametrisations of the same external time axis.

The interpretation must be stated carefully. A larger f_i does not mean that organism i possesses more biological time, but that it traverses biological time more rapidly. Thus, if $f_i > f_j$, then ϑ_i advances faster than ϑ_j with respect to the same chronological increment. The distinction between rate and total accumulated time is essential and removes the ambiguity that often appears in naive interpretations of interspecies comparisons.

9.2 Group structure and invariance

The transformation law possesses a simple algebraic structure. For three organisms i, j, and k, one finds

$$\frac{d\vartheta_i}{d\vartheta_k} = \frac{f_i}{f_k} = \frac{f_i}{f_j}\cdot\frac{f_j}{f_k}, \tag{67}$$

showing that transformations compose multiplicatively. The set of all such ratios forms a one-dimensional abelian group under multiplication, isomorphic to $(\mathbb{R}_{>0}, \times)$. This group may be interpreted as the group of metabolic time rescalings.

Within this structure, the PBTE invariant $N_\star$ plays the role of a conserved scalar. While chronological time differs between organisms and their intrinsic parametrisations differ by elements of the scaling group, the total biological arc length remains approximately invariant. In this sense, $N_\star$ is the quantity that is preserved under metabolic frame transformations, just as proper time is invariant under changes of parametrisation in relativistic kinematics.

9.3 Quantitative illustration: mouse and elephant

The transformation law acquires concrete meaning when applied to well-characterised species. For a mouse with $\bar{f}_{\mathrm{H}} \approx 600\,\mathrm{bpm}$ and an elephant with $\bar{f}_{\mathrm{H}} \approx 30\,\mathrm{bpm}$, one obtains

$$\frac{d\vartheta_{\mathrm{m}}}{d\vartheta_{\mathrm{E}}} = \frac{600}{30} = 20. \tag{68}$$

Thus, per unit chronological time, the mouse advances through biological proper time twenty times faster than the elephant.

Using the geometric relation established earlier,

$$L = \frac{N_\star}{f \times 525{,}960}, \tag{69}$$

one immediately obtains the inverse scaling of lifespans,

$$\frac{L_{\mathrm{E}}}{L_{\mathrm{m}}} \approx \frac{f_{\mathrm{m}}}{f_{\mathrm{E}}} = 20, \tag{70}$$

which yields $L_{\mathrm{E}} \approx 64\,\mathrm{yr}$ for a mouse lifespan of $3.2\,\mathrm{yr}$, in excellent agreement with observed elephant lifespans of approximately $65\,\mathrm{yr}$.

The key point is conceptual. The mouse does not experience a shorter biological lifetime in intrinsic units; rather, it traverses the same biological arc length $N_\star \sim 10^9$ at a much higher rate. The difference between species lies in the speed along the trajectory, not in the total distance covered. This is the precise meaning of the PBTE invariant within the transformation framework.

9.4 The metabolic spectrum and scaling structure

To organise the wide range of biological rates, it is useful to introduce a dimensionless scaling parameter

$$\gamma_{\mathrm{i}} = \frac{f_{\mathrm{i}}}{f_{\mathrm{ref}}}, \qquad f_{\mathrm{ref}} = 0.5\,\mathrm{Hz}, \tag{71}$$

where the reference value corresponds to the resting cardiac frequency of a large mammal such as an elephant.

The biological realisation of γ_{i} spans several orders of magnitude, from extremely slow replication cycles in viruses to rapid metabolic cycling in small endotherms. Viral systems correspond to $\gamma \sim 10^{-5}$–10^{-4}, reflecting replication times of hours to days. Bacterial systems occupy the range $\gamma \sim 10^{-3}$–10^{-2}, consistent with division times on the scale of tens of minutes to hours. Large mammals cluster near $\gamma \sim 1$, while humans lie slightly above this scale with $\gamma \sim 2$. Small mammals such as mice and shrews extend into the range $\gamma \sim 10$–10^2, reflecting their high metabolic rates.

This broad distribution defines what may be called the metabolic-temporal spectrum: a continuous scaling structure that organises biological systems according to their intrinsic rates of physiological

progression. Each organism corresponds to a trajectory parametrised by its own value of γ_i, and the ensemble of all such trajectories forms a structured region in the space of biological evolution.

9.5 The biological light-cone as an empirical envelope

The collection of all biologically realised trajectories defines a fan-shaped region in the space of chronological versus biological time. This region may be referred to as the biological light-cone. The analogy is again structural rather than literal. In relativistic physics, the light-cone defines a strict causal boundary enforced by the invariance of the speed of light. In the biological context, no such fundamental bound exists.

Instead, the biological light-cone is an empirical envelope determined by biochemical, physiological, and ecological constraints. It delineates the range of metabolic rates that are viable for living systems. Organisms within this envelope exhibit stable physiological operation, whereas trajectories that would lie far outside it are not realised in nature. Thus the biological light-cone is best understood as a domain of feasibility rather than a causal structure.

The introduction of this envelope provides a unifying picture of the metabolic spectrum. It situates individual organisms within a global structure and highlights the role of scaling laws in constraining biological diversity. At the same time, it emphasizes that the PBTE invariant operates across this entire spectrum: despite vast differences in metabolic rate, organisms traverse approximately the same intrinsic biological distance over their lifetimes.

10 Pathological Layer: The Temporal Order Parameter

10.1 Temporal order parameter and thermodynamic meaning

To quantify the progression of an organism through its intrinsic lifetime, we introduce the temporal order parameter

$$\zeta(t) = \frac{N(t)}{N_\star} = \frac{1}{N_\star}\int_0^t f(t')\,\mathrm{d}t' = \frac{\Sigma(t)}{\Sigma_\star}, \tag{72}$$

which simultaneously represents the fraction of the biological cycle budget and the fraction of the lifetime entropy budget consumed up to chronological time t. This dual representation is not coincidental; it follows directly from the thermodynamic identity $\Sigma = \sigma_0 N_\star$, and therefore encodes both kinematic and thermodynamic information in a single scalar quantity.

The interpretation is immediate. At birth, $\zeta(0) = 0$, and for a system evolving along the reference PBTE manifold one has $\zeta(L) = 1$. The value of ζ therefore provides a dimensionless measure of biological age that is intrinsic and comparable across species. Unlike chronological age, it reflects how much of the organism's thermodynamic and physiological budget has been expended.

Three qualitative regimes naturally emerge from this definition. When ζ remains close to unity at the end of life, the organism follows a homeostatic trajectory consistent with the canonical invari-

ant. When ζ exceeds unity, the organism has progressed too rapidly through its biological budget,

corresponding to accelerated aging and premature depletion of physiological resources. When ζ remains below unity, the organism has progressed more slowly, corresponding to extended longevity and delayed aging. These regimes are not arbitrary categories but direct consequences of the ratio structure defining ζ.

10.2 Empirical interpretation across physiological conditions

The order parameter provides a unified interpretation of a wide range of empirical observations. Elevated resting heart rate in mammals is well known to correlate with reduced lifespan. Within the present framework, this corresponds to an increase in the instantaneous rate $f(t)$, which causes the integral $\int_0^t f(t')\,dt'$ to grow more rapidly, driving $\zeta(t)$ toward unity at an earlier chronological time. Lifespan compression is therefore a direct consequence of accelerated traversal of biological proper time.

Chronic inflammation produces a similar effect through a different mechanism. Systemic inflammatory states elevate metabolic demand and increase entropy production, effectively increasing the rate of biological time accumulation. Epigenetic clocks, which track biological age through methylation patterns, are observed to advance more rapidly under such conditions. This can be interpreted as an increase in $d\zeta/dt$, reflecting accelerated consumption of the entropy budget.

In contrast, hibernation and torpor provide a clear example of the opposite regime. During torpor, heart rate and metabolic activity are suppressed by orders of magnitude, drastically reducing $f(t)$. As a result, biological proper time accumulates very slowly, and the chronological time required to reach $\zeta = 1$ is extended. This corresponds to $\zeta_{\text{life}} < 1$ at comparable chronological ages, placing the organism in the extended longevity regime.

These examples illustrate that $\zeta(t)$ is not merely a theoretical construct but a quantity with direct physiological interpretation across a range of biological states.

10.3 Dynamics near the reference manifold

To describe deviations from the canonical trajectory, define the fractional deviation

$$\phi(t) = \zeta(t) - \frac{t}{L_{\text{exp}}}, \tag{73}$$

which measures the difference between the actual trajectory and the reference linear progression expected under steady conditions.

Near the reference manifold, the dynamics of $\phi(t)$ may be approximated by a linear stochastic differential equation of Ornstein–Uhlenbeck type,

$$\dot{\phi}(t) = -\frac{\phi(t)}{\tau_\zeta} + \eta(t) + u(t), \tag{74}$$

where τ_ζ is a characteristic resilience timescale, $\eta(t)$ represents stochastic physiological fluctuations,

and $u(t)$ represents sustained external or internal forcing, such as chronic stress or therapeutic intervention.

The stationary power spectral density associated with this process is

$$S_\phi(\omega) = \frac{2D_\eta \tau_\zeta^2}{1 + \omega^2 \tau_\zeta^2}, \tag{75}$$

which has a Lorentzian form with characteristic frequency $\omega_c = 1/\tau_\zeta$. As the system approaches loss of stability, τ_ζ increases and the spectrum shifts toward lower frequencies, producing $1/f$-like behaviour. This provides a direct and testable prediction: physiological time series should exhibit critical slowing down as the system approaches pathological transitions.

10.4 Spatial extension and local temporal symmetry breaking

In multicellular systems, the temporal order parameter need not be uniform across space. Local tissues can evolve with intrinsic rates that differ from the organism-wide average. Introducing a spatially resolved order parameter,

$$\zeta(x, t) = \frac{f(x, t)\, \tau(x, t)}{N_\star}, \tag{76}$$

one may model its dynamics through a reaction–diffusion equation,

$$\tau_\zeta\, \partial_t \zeta = -(\zeta - 1) + D_\zeta \nabla^2 \zeta + S(x, t), \tag{77}$$

where D_ζ characterises spatial coupling and $\ell_\zeta = \sqrt{D_\zeta \tau_\zeta}$ defines a characteristic healing length.

This formulation allows a unified description of pathological phenomena as local symmetry breaking in temporal coordination. In cancer, for example, cells exhibit elevated metabolic rates and increased substrate throughput, leading to locally enhanced entropy production. This corresponds to $\zeta(x, t) \gg 1$ within tumour regions. The resulting spatial gradients disrupt coordination with surrounding tissue, contributing to loss of homeostasis and uncontrolled growth.

Viral latency represents the opposite extreme. During latency, viral replication is effectively halted, corresponding to $f_V \approx 0$ and therefore $\zeta_V \ll 1$. The viral system is essentially frozen in biological time while the host continues to evolve. Reactivation corresponds to a transition in which the local order parameter returns toward unity, restoring active progression. Therapeutic strategies such as “shock and kill” may be interpreted as controlled transitions in this temporal order parameter landscape.

10.5 Temporal phases and critical transitions

The order parameter naturally defines a phase structure. The homeostatic phase corresponds to trajectories near $\zeta \approx 1$, where regulatory mechanisms maintain stability and perturbations decay

on the timescale τ_ζ. The hypertemporal phase corresponds to $\zeta > 1$, where accelerated progression leads to premature depletion of the biological budget, as observed in chronic disease, inflammation, and advanced aging. The hypotemporal phase corresponds to $\zeta < 1$, where progression is suppressed, as in torpor, caloric restriction, or quiescent cellular states.

Near the transition between the homeostatic and hypertemporal regimes, the susceptibility

$$\chi_\zeta = \frac{\partial \langle \zeta \rangle}{\partial \Phi} \tag{78}$$

increases and the relaxation time τ_ζ diverges, signalling critical slowing down. This provides a concrete prediction: physiological time series should exhibit increased variance and long-range correlations prior to pathological transitions. Such signatures are measurable in longitudinal datasets and offer a route toward early detection of systemic instability.

10.6 Chronotherapeutic control and restoration

Restoring temporal balance may be formulated as an optimal control problem. Consider the functional

$$J[u] = \int_0^T \phi(t)^2 + \lambda u(t)^2 \, dt, \tag{79}$$

which penalises both deviation from the reference trajectory and the cost of intervention. The optimal control $u^*(t)$ takes the form of a linear feedback that drives $\phi(t)$ toward zero.

This abstract formulation has direct biological realisations. Interventions such as circadian entrainment through timed light exposure and feeding, caloric restriction, mild temperature modulation, and pharmacological targeting of metabolic pathways can all be interpreted as control inputs that modify $f(t)$ and hence $\zeta(t)$. The integration of real-time physiological monitoring with such control strategies suggests the possibility of a closed-loop chronotherapeutic system, in which the temporal order parameter is continuously estimated and regulated to maintain homeostasis.

11 The Operational Protocol: Measuring Biological Age

11.1 Individual biological clock estimation

The formal framework developed in the preceding sections becomes operational when expressed in terms of measurable physiological quantities. For an individual characterised by a lifelong mean resting heart rate $\bar{f}_H$ and current chronological age t_{now}, the accumulated biological proper time is estimated as

$$\vartheta_{acc} = \bar{f}_H \cdot t_{now} \cdot 525{,}960, \tag{80}$$

where the numerical factor converts years into minutes, ensuring consistency with the units of heart rate. This expression represents the total number of effective physiological cycles executed up to the present age under the approximation that the mean rate is representative of lifetime dynamics.

The corresponding temporal order parameter at the present age is then

$$\zeta(t_{\text{now}}) = \frac{\vartheta_{\text{acc}}}{N_\star}, \qquad N_\star = N_0 \Phi_C, \tag{81}$$

which provides a direct estimate of the fraction of the intrinsic biological and thermodynamic budget that has been consumed. This quantity is dimensionless and directly comparable across individuals and species once the appropriate clade correction Φ_C is applied.

From the same relation, one obtains an estimate of the remaining thermodynamic lifespan by solving for the time required to exhaust the remaining budget at the current physiological rate,

$$L_{\text{remaining}} = \frac{N_\star - \vartheta_{\text{acc}}}{525{,}960\, f_{\text{H}}^{\text{current}}}. \tag{82}$$

This expression highlights an important asymmetry: the accumulated biological time depends on the lifetime average rate, whereas the future trajectory depends on the current physiological state. Thus, changes in lifestyle or intervention that alter $f_{\text{H}}^{\text{current}}$ have an immediate and quantitatively predictable effect on the remaining lifespan within the PBTE framework.

11.2 Worked examples

The abstract definitions acquire concrete meaning when evaluated numerically across species and individuals.

Example 1: Comparison across species at chronological age 1 yr. Table 11 reports the biological clock fraction $\zeta(1\,\text{yr})$ for four representative species. The accumulated biological proper time over one year is given by $\vartheta(1\,\text{yr}) = \bar{f}_{\text{H}} \times 525{,}960$, and the corresponding lifetime budget $N_\star$ incorporates the clade multiplier Φ_C.

Table 11: Biological clock at chronological age 1 yr across four species. $\vartheta(1\,\text{yr}) = \bar{f}_{\text{H}} \times 525{,}960$ cycles. $N_\star = N_0 \Phi_C$ where $N_0 = 10^9$ and Φ_C is the clade multiplier from Papers 3–4. $\zeta(1) = \vartheta(1)/N_\star$ is the fraction of the lifetime thermodynamic budget consumed by chronological age 1 yr. At this single chronological age, the mouse has used 32% of its budget; the human 1%; illustrating the compression/expansion of biological time across species.

Species	$\bar{f}_{\text{H}}$ (bpm)	Φ_C	$\vartheta(1\,\text{yr})$ ($\times 10^8$)	$N_\star$ ($\times 10^9$)	$\zeta(1)$ (% used)
Mouse	600	1.0	3.15	1.00	0.315 (32%)
Dog	100	1.7	0.526	1.70	0.031 (3%)
Human	70	2.5	0.368	2.50	0.015 (1%)
Elephant	28	1.0	0.147	1.00	0.015 (1.5%)

The table makes the central conceptual point transparent. At the same chronological age, organisms are located at vastly different positions along their intrinsic biological trajectories. The mouse has

already consumed nearly one third of its lifetime budget after a single year, whereas the human has consumed only one percent. Chronological time therefore fails as a universal aging coordinate, while biological proper time provides a consistent measure across species.

Example 2: 70-year-old humans with different lifelong $\bar{f}_H$. Consider two individuals of the same chronological age but with different lifelong average heart rates. For an individual with $\bar{f}_H = 60\,\text{bpm}$, characteristic of endurance-trained physiology, one obtains

$$\vartheta_{\text{acc}} = 60 \times 70 \times 525{,}960 = 2.21 \times 10^9, \tag{83}$$

which gives $\zeta(70) = 2.21/2.5 = 0.88$ and a remaining lifespan of approximately 13 years under the current rate.

For an individual with $\bar{f}_H = 80\,\text{bpm}$, representing a chronically elevated resting heart rate, one finds

$$\vartheta_{\text{acc}} = 2.95 \times 10^9 > N_\star, \tag{84}$$

indicating that the biological budget has effectively been exhausted. This aligns with epidemiological evidence that persistently elevated resting heart rate is associated with substantially increased mortality risk. Within the PBTE framework, this is interpreted not as an isolated risk factor but as a direct manifestation of accelerated traversal of biological proper time.

12 Discussion: Biological Proper Time Framework

12.1 Biological proper time versus chronological time

The central shift introduced by the PBTE framework is the replacement of chronological time as the primary independent variable in aging analysis. Chronological time is externally defined and uniform across observers, but biological systems do not evolve uniformly with respect to it. Two organisms at the same chronological age may be at entirely different stages of their intrinsic physiological progression.

This discrepancy is not a minor correction but a structural limitation of conventional approaches. As illustrated in Table 11, a one-year-old mouse and a one-year-old human occupy radically different positions along their lifetime trajectories. Analyses that regress biological variables directly against chronological time therefore mix fundamentally incommensurate states.

The PBTE resolution is provided by the thermodynamic relation

$$\frac{d\Sigma}{d\vartheta} = \sigma_O = \text{const}, \tag{85}$$

which establishes biological proper time as the coordinate in which entropy accumulation is uniform across organisms. In this coordinate, the biological clock advances at the same thermodynamic rate

for all species. Consequently, aging biomarkers plotted against ϑ rather than chronological time should collapse onto universal curves.

The most direct empirical test arises from epigenetic clocks. If ϑ is the correct aging coordinate, methylation-based aging measures should exhibit a species-independent linear relation with slope unity in biological proper time. Existing datasets already provide partial evidence for this prediction and offer a clear path for further validation.

12.2 Interpretation of the five-layer structure

The framework is organised into five conceptual layers, each of which adds a distinct element to the theory while remaining consistent with the preceding structure.

The kinematic layer establishes the definition of biological proper time and demonstrates its empirical relevance through the lifetime invariant. It identifies the correct intrinsic coordinate but does not yet explain why this coordinate is physically privileged.

The thermodynamic layer provides that justification by showing that entropy accumulation is uniform in ϑ. This elevates the coordinate from a descriptive construct to a physically meaningful quantity tied directly to the second law of thermodynamics.

The geometric layer reveals that the invariant corresponds to the arc length of a trajectory in a well-defined metric space. This recasts the lifetime constraint as a geometric conservation law and introduces tools such as curvature and geodesics for analysing deviations.

The relativistic layer formalises the transformation properties between organisms. The ratio f_i/f_j becomes a precise Jacobian relating intrinsic clocks, and the set of such transformations forms a scaling group under which the invariant $N_\star$ is preserved.

The pathological layer introduces deviations from the reference manifold through the temporal order parameter $\zeta(t)$. It connects the abstract structure to measurable physiological quantities and predicts dynamical signatures such as critical slowing down, thereby opening a path to clinical application.

12.3 Connection to the free-energy principle

The PBTE framework naturally interfaces with existing theoretical approaches to biological organisation. In particular, Friston's free-energy principle, which posits that organisms minimise variational free energy, can be reinterpreted within the present structure. Minimising free energy corresponds, under broad conditions, to minimising excess entropy production. In the PBTE framework, this is equivalent to following geodesic trajectories in the Fisher information metric over biological proper time.

Thus the free-energy principle operates within the temporal and thermodynamic substrate defined by PBTE. The former describes how organisms regulate their internal models, while the latter

specifies the intrinsic temporal coordinate and energetic constraints under which that regulation occurs.

12.4 Limitations and scope

The current formulation has several limitations that define its scope. The canonical metric $\varphi(f) = f^2$ treats all physiological cycles equally, neglecting variation in metabolic intensity across different states such as rest and exertion. A more refined formulation would weight cycles by their entropy cost, requiring detailed metabolic measurements.

The estimation of $\zeta(t)$ at the individual level depends on accurate heart-rate data over extended periods. While modern wearable devices provide sufficient precision for practical applications, population-level datasets based on averaged values may obscure important temporal variations.

Finally, the extension of the framework beyond endothermic vertebrates remains an open problem. While the transformation law and scaling structure can be formally extended to microorganisms and viruses, the empirical validation of a strict lifetime invariant in these domains is currently limited and requires dedicated investigation.

13 Synthesis: Biological Proper Time

Biological proper time $\vartheta_i(t) = \int_0^t f_i(t')\,\mathrm{d}t'$ emerges, within the present framework, not as a convenient redefinition of chronological time but as the intrinsic temporal coordinate that organises the dynamics of living systems. It is a measurable, dimensionless observable whose structure, when examined across the five formal layers developed in this work, reveals the organism as a thermodynamic system evolving along a trajectory constrained by a finite dissipative budget.

At the kinematic level, ϑ_i is invariant under reparametrisation of chronological time and is directly measurable through integration of physiological rates such as heart frequency. Its most striking empirical property is developmental universality: major life-history events—sexual maturity, onset of senescence, and peak reproductive capacity—occur at approximately fixed fractions of the normalised coordinate $\hat{\vartheta}_i \in [0, 1]$ across species whose chronological lifespans differ by orders of magnitude. This universality, which is completely obscured in chronological time, provides the first empirical indication that ϑ is the appropriate biological clock.

At the thermodynamic level, the PBTE closure $\dot{e}_p = \sigma_0 f_i$ implies that entropy production becomes uniform when expressed in biological proper time. The relation $\mathrm{d}\Sigma/\mathrm{d}\vartheta = \sigma_0 = \mathrm{const}$ holds independently of metabolic rate, making ϑ the unique temporal coordinate in which the entropy budget of an organism is linearly accumulated. This uniqueness elevates biological proper time from a descriptive parameter to a physically privileged observable. The resulting distinction between Class 1 mechanisms, which alter the rate of traversal of ϑ, and Class 2 mechanisms, which alter the entropy cost per cycle, provides a direct and experimentally accessible test using longitudinal epigenetic datasets.

At the geometric level, the lifetime invariant $N_\star \approx 10^9$ is identified with the arc length of the organism's trajectory in the biological metric $\mathrm{d}s_i^2 = f_i^2(t)\,\mathrm{d}t^2$. The invariance of $N_\star$ is therefore not merely empirical but reflects a geometric conservation law. The introduction of the nonstationarity index $R_i(t)$ provides a diagnostic of temporal curvature in the trajectory, allowing identification of physiological instability without direct calorimetric measurement of σ_O. The extension to information geometry through the Fisher metric further links the framework to optimal regulation, where geodesic trajectories minimise excess entropy production.

At the relativistic level, the transformation law $\mathrm{d}\vartheta_i/\mathrm{d}\vartheta_j = f_i/f_j$ defines an abelian scaling group acting on biological time. The invariant $N_\star$ appears as the conserved scalar under this group, establishing a symmetry principle underlying the PBTE framework. The metabolic-temporal spectrum, spanning organisms from viruses to whales, defines an empirical envelope of feasible biological rates. The analogy to a light-cone is structural: it organises the space of trajectories but does not impose a fundamental causal limit.

At the pathological level, the temporal order parameter $\zeta(t) = N(t)/N_\star$ provides a unifying description of aging, disease, and intervention. Hypertemporal states, characterised by $\zeta > 1$, correspond to accelerated consumption of the biological budget and include chronic inflammation, cancer, and premature aging. Hypotemporal states, with $\zeta < 1$, correspond to suppressed metabolic activity and include torpor, caloric restriction, and viral latency. The Ornstein–Uhlenbeck dynamics of deviations from the reference trajectory predict measurable spectral signatures, including critical slowing down near transitions. The formulation of chronotherapy as an optimal-control problem provides a direct pathway from theory to practical intervention.

The central contribution of this work is therefore not a single result but the identification of a coherent structure linking empirical regularity, thermodynamic constraint, geometric interpretation, symmetry principle, and pathological deviation. An organism does not simply exist for a number of years; it evolves along a thermodynamically defined worldline of fixed arc length, traversed at a rate determined by its physiology and modifiable by environmental and biological factors.

Two predictions follow directly from this structure. First, epigenetic aging clocks, when expressed in biological proper time, should collapse onto a universal relation with slope unity across mammalian species. Second, Class 1 and Class 2 interventions should produce distinguishable signatures in aging rates measured per physiological cycle, providing a clear experimental test of the framework.

14 The Untested Assumption and the Required Experiment

The central limitation of the PBTE framework lies in the current status of its key closure assumption. The approximate constancy of σ_0^* is inferred from the observed constancy of $N_\star$, leading to a circular logical structure in which the explanation relies on the phenomenon it seeks to explain. This circularity cannot be resolved by allometric consistency arguments or theoretical plausibility alone.

A decisive test requires direct and independent measurement of the relevant quantities across species.

Specifically, simultaneous measurements of metabolic power P_i, physiological frequency f_i, body temperature T_i, and body mass M_i must be obtained for a sufficiently large and diverse set of species. The quantity $\sigma_0^* = P_i/(T_i f_i M_i)$ is then computed independently for each species, and its dependence on body mass is tested statistically.

If σ_0^* is found to be mass-independent within experimental uncertainty, the closure assumption is validated and the PBTE framework acquires the status of a genuine physical explanation. If significant scaling is observed, the closure must be revised and the invariant reinterpreted. Until such measurements are performed, the framework remains a thermodynamically motivated and internally consistent parametrisation supported by empirical concordance but not yet fully validated as a fundamental law.

15 Discussion

The dimensional analysis leading to $\sigma_0^* \propto M^0$ is straightforward, but the PBTE framework extends far beyond this observation. It provides a physical interpretation of σ_0^* as the entropy cost per physiological cycle, introduces a closure relation linking entropy production to physiological rate, establishes a thermodynamic identity connecting lifetime cycle count to dissipative budget, and defines biological proper time as a universal coordinate for physiological processes.

It further introduces a hierarchical structure explaining the limits of classical scaling laws, provides predictive relations for lifespan interventions, and connects entropy accumulation to aging dynamics consistent with observed mortality laws. These elements collectively form a coherent theoretical framework that cannot be reduced to dimensional analysis alone.

The concept of biological proper time relates to earlier notions of physiological time but is distinguished by its explicit connection to entropy production. This connection gives the invariant a physical foundation and transforms it from an empirical observation into a thermodynamic principle.

Nevertheless, limitations remain. The closure assumption has not been independently verified, the allometric exponents are taken as empirical inputs, and certain clade-specific mechanisms remain only partially explained. The aging model, while consistent with observed patterns, remains phenomenological pending a detailed microscopic derivation.

16 Conclusions

We have developed a thermodynamically grounded framework for the vertebrate lifetime cycle invariant $N_\star \approx 10^9$. The central relation $N_\star = \Sigma/\sigma_0$ interprets lifetime as a dissipative budget divided by an entropy cost per cycle, and biological proper time $\vartheta_i(t) = \int_0^t f_i \, dt'$ emerges as the intrinsic coordinate governing this process.

The invariance of $N_\star$ reflects a balance between metabolic rate and lifespan, such that all organisms traverse approximately the same biological distance regardless of chronological duration. Devia-

tions from this invariant encode meaningful biological mechanisms and provide a framework for understanding aging, disease, and intervention.

The theory makes clear, testable predictions and identifies the key experiment required for validation. Its structure integrates empirical regularities, thermodynamic constraints, geometric interpretation, and dynamical modeling into a unified description of biological time.

Methods

Numerical estimates. All calculations use Kleiber's law [13] $P = 3.4\,M^{0.75}$ W, Calder cardiac allometry [14] $f = 241\,M^{-0.25}$ bpm $= 4.017\,M^{-0.25}$ Hz, and $T = 310$ K throughout, yielding $\sigma_0^* = 2.73 \times 10^{-3}$ J K^{-1} beat^{-1} kg^{-1}. The empirical mean $\sigma_0^* = (3.0 \pm 0.5) \times 10^{-3}$ from Table 2 is adopted for all numerical predictions, giving $N_0 \approx 1.52 \times 10^9$.

Data sources. Species heart-rate and lifespan data from the AnAge database [28, 5]. Body temperatures from Schmidt-Nielsen (1984) [14]. Bird allometric parameters from Calder [14] and Prinzinger et al. [29]. Primate metabolic suppression factor from Pontzer et al. [15, 19]. Proton-leak fractions from Hulbert et al. [16] and Brand et al. [30]. Cetacean dive heart-rate data from Goldbogen et al. [31] and Williams et al. [32].

Phylogenetically independent contrasts (PIC). PIC analysis used the Felsenstein [33] method (ape::pic() in R 4.3) on the Bininda-Emonds mammal supertree [34], pruned to the 112 endotherm species in the dataset. PIC regression was fitted through the origin as required by the method.

Arrhenius correction. Ectotherm heart rates were corrected to $T_{\mathrm{ref}} = 310$ K using $f_{\mathrm{H}}^{\mathrm{corr}} = f_{\mathrm{H}}^{\mathrm{raw}} \exp[(E_a/k_B)(1/T_{\mathrm{field}} - 1/T_{\mathrm{ref}})]$ with $E_a = 0.65$ eV following Gillooly et al. [35].

Simulated figures. Figure 2 (biological proper time trajectories) and Figure 8 (epigenetic clock schematic) use theoretical parameter values; no statistical conclusions should be drawn from them. Figure 5 uses real species data from AnAge. All simulated scatter uses fixed random seed (seed = 42).

Data availability. No new data were generated in this study.

Competing interests. None declared.

Acknowledgements. [To be completed.]

References

[1] M. Rubner, *Das Problem der Lebensdauer* (Oldenbourg, Munich, 1908).

[2] S. L. Lindstedt and W. A. Calder, Q. Rev. Biol. **56**, 1 (1981).

[3] S. D. Livingstone and L. A. Kuehn, Aviat. Space Environ. Med. **50**, 1037 (1979).

[4] H. J. Levine, J. Am. Coll. Cardiol. **30**, 1104 (1997).

[5] M. A. Taye, J. R. Soc. Interface (submitted 2026). [The empirical lifetime cycle invariant of endothermic vertebrates: a 230-species comparative dataset, statistical validation, and falsifiability criteria.] The complete species dataset underlying all statistical results cited from this reference is reproduced in Appendix B of the present paper and can be verified independently.

[6] G. B. West, J. H. Brown, and B. J. Enquist, Science **276**, 122 (1997).

[7] D. S. Glazier, Proc. R. Soc. B **289**, 20221605 (2022).

[8] R. Pearl, *The Rate of Living* (Knopf, New York, 1928).

[9] J. R. Speakman, J. Exp. Biol. **208**, 1717 (2005).

[10] I. Prigogine, *Introduction to Thermodynamics of Irreversible Processes*, 3rd ed. (Wiley-Interscience, New York, 1967).

[11] U. Seifert, Rep. Prog. Phys. **75**, 126001 (2012).

[12] E. Schrödinger, *What Is Life?* (Cambridge University Press, Cambridge, 1944).

[13] M. Kleiber, Hilgardia **6**, 315 (1932).

[14] W. A. Calder, *Size, Function, and Life History* (Harvard University Press, Cambridge, MA, 1984).

[15] H. Pontzer *et al.*, Proc. Natl Acad. Sci. USA **111**, 1433 (2014).

[16] A. J. Hulbert *et al.*, Physiol. Rev. **87**, 1175 (2007).

[17] R. J. Colman *et al.*, Nat. Commun. **5**, 3557 (2014).

[18] S. Herculano-Houzel, PLOS ONE **6**, e17514 (2011).

[19] A. K. Yegian *et al.*, Proc. Natl Acad. Sci. USA **121**, e2313703121 (2024).

[20] K. Friston, Nat. Rev. Neurosci. **11**, 127 (2010).

[21] G. S. Wilkinson and J. M. South, Aging Cell **1**, 124 (2002).

[22] G. Barja and A. Herrero, J. Bioenerg. Biomembr. **30**, 235 (1998).

[23] C. E. Ogburn *et al.*, J. Gerontol. A **56**, B468 (2001).

[24] S. R. Noren and T. M. Williams, J. Exp. Biol. **203**, 3601 (2000).

[25] B. Gompertz, Phil. Trans. R. Soc. Lond. **115**, 513 (1825).

[26] S. Horvath, Genome Biol. **14**, R115 (2013).

[27] M. Belánger *et al.*, Ann. N.Y. Acad. Sci. (in press, 2025).

[28] Human Ageing Genomic Resources, *AnAge build 15* (2023), https://genomics.senescence.info/species/.

[29] R. Prinzinger, A. Präsmar, and E. Schleucher, Comp. Biochem. Physiol. A **99**, 499 (1991).

[30] M. D. Brand *et al.*, Biochem. J. **392**, 353 (2000).

[31] J. A. Goldbogen *et al.*, Proc. Natl Acad. Sci. USA **116**, 25329 (2019).

[32] T. M. Williams *et al.*, Nat. Commun. **6**, 6055 (2015).

[33] J. Felsenstein, Am. Nat. **125**, 1 (1985).

[34] O. R. P. Bininda-Emonds *et al.*, Nature **446**, 507 (2007).

[35] J. F. Gillooly *et al.*, Science **293**, 2248 (2001).

[36] K. E. Jones *et al.*, Ecology **90**, 2648 (2009).

[37] C. P. Lyman *et al.*, *Hibernation and Torpor in Mammals and Birds* (Academic Press, New York, 1982).

[38] P. Uetz *et al.*, *The Reptile Database* (2023), http://www.reptile-database.org/.

[39] K. A. Christian and B. W. Weavers, Copeia **1999**, 688 (1999).

[40] A. Clarke and P. Rothery, Funct. Ecol. **22**, 58 (2008).

[41] Taye, M.A. (2026) *The Principle of Biological Time Equivalence*. West Los Angeles College [in preparation].

[42] Taye, M.A. (2026) Neural investment as an entropy-budget strategy. *J. Theor. Biol.* [submitted].

[43] Taye, M.A. (2026) Three physiological strategies, one invariant. *Proc. R. Soc. B* [submitted].

[44] Ruf, T. & Geiser, F. (2015) Daily torpor and hibernation. *Biol. Rev.* **90**, 891–926.

[45] Warburg, O. (1956) On the origin of cancer cells. *Science* **123**, 309–314.

Appendix A. Detailed Derivation of the Entropy Cost per Beat and the Cycle-Count Scaling Law

This appendix gives a detailed derivation of the entropy-per-beat representation, the lifetime cycle-count relation, and the power-law dependence of lifetime cardiac cycles on the control parameter ϕ. The purpose is to make explicit each mathematical step connecting the instantaneous entropy production rate to the total lifetime cycle budget.

A.1. Instantaneous entropy production and change of variable from time to beat count

Let t denote chronological time and let n denote the cumulative cardiac cycle count. The cardiac frequency is

$$f_{\mathrm{H}}(t) = \frac{dn}{dt}, \tag{86}$$

so that

$$dn = f_{\mathrm{H}}(t)\, dt, \qquad dt = \frac{dn}{f_{\mathrm{H}}}. \tag{87}$$

Here f_{H} has units of cycles per unit time. Let $\sigma(t)$ be the instantaneous entropy production rate, with units of entropy per unit time. The total entropy produced over an infinitesimal interval dt is

$$d\Sigma = \sigma(t)\, dt. \tag{88}$$

Using (87), we rewrite this increment in terms of the beat-count variable:

$$d\Sigma = \sigma(t)\, \frac{dn}{f_{\mathrm{H}}(t)}. \tag{89}$$

If we regard both σ and f_{H} as functions of the cycle-count coordinate n, then

$$d\Sigma = \frac{\sigma(n)}{f_{\mathrm{H}}(n)}\, dn. \tag{90}$$

This motivates the definition of the entropy cost per beat at cycle index n:

$$\sigma_{\mathrm{O}}(n) \equiv \frac{\sigma(n)}{f_{\mathrm{H}}(n)}. \tag{91}$$

The dimensional consistency is immediate:

$$[\sigma] = \frac{\text{entropy}}{\text{time}}, \qquad [f_{\mathrm{H}}] = \frac{\text{cycles}}{\text{time}}, \qquad \frac{\sigma}{f_{\mathrm{H}}} = \frac{\text{entropy/time}}{\text{cycles/time}} = \frac{\text{entropy}}{\text{cycle}}.$$

Thus $\sigma_{\mathrm{O}}(n)$ is the entropy production associated with one cardiac cycle.

A.2. Total lifetime entropy production as a sum over beats

Suppose that the organism experiences a total of N cardiac cycles over its lifetime. Then the total lifetime entropy production is obtained by integrating (90) from the first to the last cycle:

$$\Sigma_{\mathrm{life}} = \int_0^N d\Sigma = \int_0^N \sigma_{\mathrm{O}}(n)\, dn. \tag{92}$$

Equation (92) is simply the beat-count analogue of summing the entropy cost incurred at each cycle.

Since the beat-count variable is treated continuously, the sum is represented as an integral.

We now define the lifetime mean entropy cost per beat:

$$\langle \sigma_O \rangle \equiv \frac{1}{N} \int_0^N \sigma_O(n)\, dn. \tag{93}$$

Using (92), this immediately gives

$$\Sigma_{life} = N \langle \sigma_O \rangle . \tag{94}$$

Substituting the explicit definition (91) into (93), we may also write

$$\langle \sigma_O \rangle = \frac{1}{N} \int_0^N \frac{\sigma(n)}{f_H(n)}\, dn. \tag{95}$$

Equation (94) has a direct interpretation: the total lifetime entropy production equals the total number of beats multiplied by the mean entropy cost of one beat.

For species *i*, the corresponding notation is

$$\sigma_{O,i} \equiv \frac{1}{N_i^\star} \int_0^{N_i^\star} \sigma_O(n)\, dn, \tag{96}$$

so that

$$\Sigma_i = N_i^\star \sigma_{O,i}, \tag{97}$$

where Σ_i (J K^{-1}) is total lifetime entropy production and $\sigma_{O,i}$ (J K^{-1} $beat^{-1}$) is entropy per cycle.

A.3. Lifetime entropy budget and the fundamental cycle-count relation

The central hypothesis is that the lifetime entropy production is approximately constrained by a characteristic budget $\Sigma_\star$:

$$\Sigma_{life} \approx \Sigma_\star. \tag{98}$$

Combining (94) with (98) yields

$$N \langle \sigma_O \rangle \approx \Sigma_\star. \tag{99}$$

Solving for N, we obtain the fundamental cycle-count relation:

$$N = \frac{\Sigma_\star}{\langle \sigma_O \rangle}. \tag{100}$$

For species *i*, the lifetime cycle count is

$$N_i^\star = \frac{\Sigma_i}{\sigma_{O,i}}. \tag{101}$$

where Σ_i (J K^{-1}) is total lifetime entropy production and $\sigma_{0,i}$ (J K^{-1} $beat^{-1}$) is entropy per cycle.

This expression states that the total number of cardiac cycles that can occur over the lifetime is inversely proportional to the average entropy cost of each beat, given a fixed lifetime entropy budget. A lower entropy cost per beat permits more cycles within the same budget, whereas a higher cost per beat permits fewer cycles.

A.4. Baseline calibration and mammalian reference value

Let ϕ_0 denote a baseline reference state and let N_0 be the corresponding reference total number of lifetime cardiac cycles. Evaluating (100) at the baseline gives

$$N_0 = \frac{\Sigma_\star}{\langle \sigma_0 \rangle_0}, \tag{102}$$

where

$$\langle \sigma_0 \rangle_0 \equiv \langle \sigma_0(\phi_0) \rangle . \tag{103}$$

Rearranging (102) gives the baseline entropy cost per beat:

$$\langle \sigma_0 \rangle_0 = \frac{\Sigma_\star}{N_0} . \tag{104}$$

Equation (104) provides the calibration point from which the dependence on ϕ is measured.

A.5. Logarithmic sensitivity of the entropy cost per beat

We now introduce a control parameter ϕ that modulates the mean entropy cost per beat through multiple mechanisms. The hypothesis is that increasing ϕ reduces $\langle \sigma_0 \rangle$. To quantify this response, define the logarithmic sensitivity at the baseline:

$$\alpha \equiv - \left. \frac{\partial \ln \langle \sigma_0 \rangle}{\partial \ln \phi} \right|_{\phi=\phi_0} . \tag{105}$$

The derivative

$$\frac{\partial \ln \langle \sigma_0 \rangle}{\partial \ln \phi} = \frac{\phi}{\langle \sigma_0 \rangle} \frac{\partial \langle \sigma_0 \rangle}{\partial \phi}$$

is the elasticity of the entropy cost per beat with respect to ϕ, that is, the fractional change in $\langle \sigma_0 \rangle$ induced by a fractional change in ϕ. Since the response is assumed monotonic and decreasing, the derivative is negative; the minus sign in (105) ensures that $\alpha > 0$.

If three independent reduction channels contribute multiplicatively to the decrease of $\langle \sigma_0 \rangle$, with logarithmic sensitivities γ_1, γ_2, and γ_3, then the aggregate sensitivity is additive:

$$\alpha = \gamma_1 + \gamma_2 + \gamma_3 > 0. \tag{106}$$

The reason is straightforward. If

$$\langle \sigma_O \rangle \propto \phi^{-\gamma_1} \phi^{-\gamma_2} \phi^{-\gamma_3}, \tag{107}$$

then

$$\langle \sigma_O \rangle \propto \phi^{-(\gamma_1+\gamma_2+\gamma_3)}, \tag{108}$$

and therefore

$$-\frac{\partial \ln \langle \sigma_O \rangle}{\partial \ln \phi} = \gamma_1 + \gamma_2 + \gamma_3. \tag{109}$$

A.6. Integration of the logarithmic sensitivity and the power-law form

Equation (105) defines the local logarithmic slope at the baseline ϕ_0. To obtain a finite-range scaling law, we assume that this logarithmic response remains approximately constant over the interval of interest. This is the scale-free power-law approximation commonly used in allometric analysis. Under this assumption,

$$-\frac{d \ln \langle \sigma_O \rangle}{d \ln \phi} = \alpha, \tag{110}$$

or equivalently,

$$d \ln \langle \sigma_O \rangle = -\alpha \, d \ln \phi. \tag{111}$$

We now integrate from the baseline ϕ_0, where $\langle \sigma_O \rangle = \langle \sigma_O \rangle_O$, to a general value ϕ:

$$\int_{\ln \phi_0}^{\ln \phi} d \ln \langle \sigma_O \rangle = -\alpha \int_{\ln \phi_0}^{\ln \phi} d \ln \phi. \tag{112}$$

This gives

$$\ln \langle \sigma_O(\phi) \rangle - \ln \langle \sigma_O \rangle_O = -\alpha \, (\ln \phi - \ln \phi_0). \tag{113}$$

Combining the logarithms,

$$\ln \frac{\langle \sigma_O(\phi) \rangle}{\langle \sigma_O \rangle_O} = -\alpha \ln \frac{\phi}{\phi_0}. \tag{114}$$

Exponentiating both sides yields the power-law form:

$$\langle \sigma_O(\phi) \rangle = \langle \sigma_O \rangle_O \left(\frac{\phi}{\phi_0} \right)^{-\alpha}. \tag{115}$$

Equation (115) states that the mean entropy cost per beat decreases as a power law in ϕ, with exponent $\alpha > 0$.

A.7. Consequence for total lifetime cardiac cycles

Substituting (115) into the cycle-count relation (100) gives

$$N(\phi) = \frac{\Sigma_\star}{\langle \sigma_O(\phi) \rangle} = \frac{\Sigma_\star}{\langle \sigma_O \rangle_O \left(\frac{\phi}{\phi_O} \right)^{-\alpha}}. \tag{116}$$

Using the baseline identity (104),

$$\frac{\Sigma_\star}{\langle \sigma_O \rangle_O} = N_O,$$

we obtain

$$N(\phi) = N_O \left(\frac{\phi}{\phi_O} \right)^{\alpha}. \tag{117}$$

Thus, under the fixed lifetime entropy-budget hypothesis, any systematic reduction in the entropy cost per beat produces a corresponding increase in the total number of lifetime cardiac cycles. The scaling exponent governing this increase is the same aggregate sensitivity α that governs the decrease of the entropy cost per beat.

A.8. Interpretation of the result

The derivation shows that the lifetime cycle count is controlled by two ingredients: a finite lifetime entropy budget $\Sigma_\star$ and an average entropy expenditure per cycle $\langle \sigma_O \rangle$. Once the budget is fixed, the total number of admissible cycles is determined entirely by how costly each cycle is in entropic terms. A reduction in entropy cost per beat allows a larger number of beats to be accommodated within the same total budget. If the reduction is scale-free in ϕ, then the increase in cycle count is likewise scale-free.

In compact form, the chain of reasoning is

$$d\Sigma = \sigma \, dt = \frac{\sigma}{f_H} dn, \qquad \sigma_O = \frac{\sigma}{f_H}, \qquad \Sigma_{life} = \int_0^N \sigma_O(n) \, dn = N \langle \sigma_O \rangle, \tag{118}$$

together with

$$\Sigma_{life} \approx \Sigma_\star \Rightarrow N = \frac{\Sigma_\star}{\langle \sigma_O \rangle}, \tag{119}$$

and

$$\langle \sigma_O(\phi) \rangle = \langle \sigma_O \rangle_O \left(\frac{\phi}{\phi_O} \right)^{-\alpha} \Rightarrow N(\phi) = N_O \left(\frac{\phi}{\phi_O} \right)^{\alpha}. \tag{120}$$

For species i, this compact relation becomes

$$\Sigma_i = N_i^\star \sigma_{O,i}, \qquad N_i^\star = \frac{\Sigma_i}{\sigma_{O,i}}, \tag{121}$$

where Σ_i (J K^{-1}) is total lifetime entropy production and $\sigma_{O,i}$ (J K^{-1} $beat^{-1}$) is entropy per cycle.

A.9. Assumptions used in the derivation

For clarity, the derivation rests on the following assumptions.

First, the cardiac cycle count n is treated as a continuous variable, which is appropriate when the total number of cycles is very large.

Second, the lifetime entropy production is assumed to be well approximated by a characteristic budget $\Sigma_\star$.

Third, the response of the entropy cost per beat to the control parameter ϕ is assumed to be monotonic and approximately scale-free over the range of interest, so that the logarithmic sensitivity may be treated as approximately constant.

Fourth, the different contributing channels are taken to combine multiplicatively, which leads to additive logarithmic sensitivities.

Within these assumptions, the power-law result (117) follows directly and rigorously from the entropy-budget framework.

Appendix B. Complete 230-Species Dataset

The following tables contain the complete dataset of 230 adult vertebrate species used in all analyses. All ℓ values are computed as $\ell = \log_{10}(f_H^{\mathrm{eff}} \times L \times 525{,}960)$ directly from the f_H^{eff} and L columns and have been verified internally consistent. A tab-delimited machine-readable version is available from the corresponding author on request.

Column definitions. M : adult body mass (kg). f_H (bpm): resting (or duty-corrected/Arrhenius-corrected) heart rate. T (K): mean core (endotherms) or field (ectotherms) body temperature. L (yr): maximum recorded natural lifespan (AnAge build 15 [28]). ℓ: PBTE invariant = $\log_{10}(f_H^{\mathrm{eff}} \times L \times 525{,}960)$. Corr.: correction applied (– = none; TA = torpor-cycle average; DA = dive-cycle average; AQ = Arrhenius correction to $T_{\mathrm{ref}} = 310$ K). † = heart rate allometrically imputed from $f_H = 241 M^{-0.25}$ bpm [14]. Sources: A = AnAge [28]; P = PanTHERIA [36]; C = Calder (1984) [14]; Pr = Prinzinger et al. (1991) [29]; L = Lyman et al. (1982) [37]; Ch = Christian & Weavers (1999) [39]; U = Uetz et al. (2023) [38]; G = Goldbogen et al. (2019) [31]; Cl = Clarke & Rothery (2008) [40].

B.1 Non-primate placental mammals (n = 46)

Table 12: Non-primate placentals. Clade mean $\bar{\ell}$ = 8.995 ± 0.160 (n = 46).

Species	M (kg)	f_H (bpm)	T (K)	L (yr)	ℓ	Source
Suncus etruscus	0.002	835	310.5	1.5	8.82	C
Sorex araneus	0.010	1000	310.5	3.3	9.24	C,A
Mus musculus	0.022	632	310.0	3.5	9.07	A,C
Rattus norvegicus	0.280	420	310.0	3.8	8.92	A,P
Mesocricetus auratus	0.130	450	310.5	3.9	8.97	A,P
Meriones unguiculatus	0.060	400	310.0	5.0	9.02	A,P
Cavia porcellus	0.750	270	310.0	7.1	9.00	A,P
Sciurus carolinensis	0.520	310	310.0	12.0	9.29	A,P
Lepus europaeus	3.5	220	310.0	12.5	9.16	A,P
Oryctolagus cuniculus	2.2	205	310.0	9.0	8.99	A,C
Felis catus	4.1	150	310.5	15.0	9.07	A,P
Mustela putorius	1.0	280	310.5	5.0	8.87	A,P
Martes martes	1.2	245	310.5	17.0	9.34	A,P
Vulpes vulpes	6.8	120	310.5	14.0	8.95	A,P
Canis lupus familiaris	23	90	310.5	20.0	8.98	A,P
Ursus arctos	220	50	310.5	47.0	9.09	A,P
Ovis aries	63	75	310.0	20.0	8.90	A,P
Capra hircus	45	80	310.5	18.0	8.88	A,P
Sus scrofa	100	70	310.5	27.0	9.00	A,P
Bos taurus	500	55	310.5	25.0	8.86	A,P
Equus caballus	500	38	310.5	46.0	8.96	A,C
Equus asinus	250	44	310.5	47.0	9.04	A,P
Rhinoceros unicornis	2100	30†	310.5	47.0	8.87	A
Tapirus terrestris	240	42	310.5	35.0	8.89	A,P
Loxodonta africana	4000	28	310.5	65.0	8.98	A,P
Elephas maximus	4000	27	310.5	86.0	9.09	A,P
Hippopotamus amphibius	1500	55	310.5	55.0	9.20	A,P
Giraffa camelopardalis	900	65	310.5	39.5	9.13	A,P
Cervus elaphus	200	60	310.5	26.8	8.93	A,P
Rangifer tarandus	110	65	310.0	20.0	8.83	A,P
Trichechus manatus	500	50	310.5	59.0	9.19	A,P
Dugong dugon	400	52†	310.5	73.0	9.30	A
Procavia capensis	3.5	230	310.5	12.0	9.16	A,P
Erinaceus europaeus	0.80	310	310.0	10.0	9.21	A,P
Talpa europaea	0.080	350	310.0	3.5	8.81	A,P
Orycteropus afer	65	70†	310.5	24.0	8.95	A
Ondatra zibethicus	1.4	280	310.0	5.0	8.87	A,P
Castor canadensis	20	150	310.0	24.0	9.28	A,P
Hydrochoerus hydrochaeris	55	70	310.0	12.0	8.65	A,P
Myocastor coypus	7.0	155	310.0	9.0	8.87	A,P
Lepus californicus	2.2	215	310.0	8.0	8.96	A,P
Ochotona princeps	0.160	300	310.0	6.0	8.98	A,P
Panthera leo	180	50	310.5	29.0	8.88	A,P
Panthera tigris	260	46	310.5	26.0	8.80	A,P
Acinonyx jubatus	54	60	310.5	14.9	8.67	A,P
Panthera pardus	70	55	310.5	23.0	8.82	A,P

B.2 Primates (n = 18)

Table 13: Primates. Clade mean $\bar{\ell} = 9.376 \pm 0.125$ (n = 18). $\phi = P_{\text{brain}}/P_{\text{body}}$.

Species	M (kg)	f_H (bpm)	T (K)	L (yr)	ℓ	ϕ	Source
Callithrix jacchus	0.35	220	309.5	16.5	9.28	0.06	A,P
Saimiri sciureus	0.77	195	309.5	30.2	9.49	0.07	A,P
Aotus trivirgatus	0.79	185	309.5	25.0	9.39	0.07	A,P
Cebus capucinus	3.3	150	309.5	54.0	9.63	0.09	A,P
Lemur catta	2.2	165	309.5	37.3	9.51	0.05	A,P
Propithecus verreauxi	3.4	145	309.5	30.0	9.36	0.05	A,P
Daubentonia madagascariensis	2.7	155	309.5	23.3	9.28	0.06	A,P
Macaca mulatta	7.7	120	309.0	40.0	9.40	0.07	A,P
Macaca fascicularis	5.4	130	309.0	39.0	9.43	0.07	A,P
Theropithecus gelada	18	95	309.0	30.0	9.18	0.08	A,P
Papio ursinus	25	90	309.0	45.0	9.33	0.08	A,P
Colobus guereza	10	110	309.0	30.0	9.24	0.07	A,P
Hylobates lar	5.7	100	308.5	44.0	9.36	0.10	A,P
Pongo pygmaeus	73	65	307.5	58.7	9.30	0.10	A,P
Gorilla gorilla	160	60	307.0	55.4	9.24	0.09	A,P
Pan troglodytes	50	75	307.0	59.4	9.37	0.12	A,P
Pan paniscus	35	80	307.0	50.0	9.32	0.12	A,P
Homo sapiens	70	70	306.5	122.5	9.65	0.20	A

B.3 Marsupials and monotremes ($n = 19$)

Table 14: Marsupials and monotremes. Clade mean $\bar{\ell} = 8.933 \pm 0.204$ ($n = 19$).

Species	M (kg)	f_H (bpm)	T (K)	L (yr)	ℓ	Source
Didelphis virginiana	2.3	180	308.5	4.5	8.63	A,P
Monodelphis domestica	0.080	450	308.5	3.3	8.89	A,P
Macropus rufus	30	80	309.0	22.3	8.97	A,P
Macropus giganteus	27	82	309.0	19.0	8.91	A,P
Wallabia bicolor	16	100	309.0	15.0	8.90	A,P
Trichosurus vulpecula	2.1	160	308.5	13.0	9.04	A,P
Petaurus breviceps	0.14	300	308.0	10.0	9.20	A,P
Vombatus ursinus	28	90	309.0	26.0	9.09	A,P
Phascolarctos cinereus	8.5	100	308.5	18.0	8.98	A,P
Perameles gunnii	0.90	190	308.5	3.2	8.50	A,P
Dasyurus viverrinus	1.2	200	308.5	4.5	8.68	A,P
Sarcophilus harrisii	8.0	130	308.5	7.5	8.71	A,P
Myrmecobius fasciatus	0.44	245	307.5	5.6	8.86	A
Sminthopsis crassicaudata	0.018	580	307.5	5.0	9.18	A,P
Notoryctes typhlops	0.055	440†	307.5	3.0	8.84	A
Tachyglossus aculeatus	4.0	70	305.0	49.5	9.26	A,P
Ornithorhynchus anatinus	1.5	140	307.5	21.0	9.19	A,P
Zaglossus bruijni	10	60†	305.0	37.0	9.07	A
Bettongia penicillata	1.1	210	308.5	6.0	8.82	A,P

B.4 Bats (Chiroptera, $n = 31$)

For bats, f_H is the measured active-phase rate; f_H^{avg} is the duty-cycle-corrected time-average used in ℓ, with q the annual torpor fraction [37].

Table 15: Bats. Clade mean $\bar{\ell} = 9.540 \pm 0.163$ ($n = 31$, duty-corrected). Corr. TA = torpor-cycle average applied.

Species	M (g)	f_H (bpm)	q	f_H^{avg} (bpm)	L (yr)	ℓ	Corr.
Myotis lucifugus	8	600	0.50	305	34.0	9.74	TA
Myotis myotis	28	550	0.48	282	37.0	9.74	TA
Myotis daubentonii	9	580	0.48	296	40.0	9.79	TA
Myotis brandtii	6	620	0.50	315	41.0	9.83	TA
Eptesicus fuscus	18	550	0.45	310	19.0	9.49	TA
Eptesicus serotinus	18	545	0.45	308	21.0	9.53	TA
Rhinolophus ferrumequinum	19	550	0.48	282	30.0	9.65	TA
Rhinolophus hipposideros	7	600	0.48	307	30.5	9.69	TA
Plecotus auritus	9	600	0.50	305	30.0	9.68	TA
Corynorhinus townsendii	11	580	0.50	295	30.0	9.67	TA
Perimyotis subflavus	5	630	0.50	320	14.6	9.39	TA
Tadarida brasiliensis	13	600	0.30	425	11.0	9.39	TA
Pteronotus parnellii	19	550	0.20	452	10.0	9.38	TA
Desmodus rotundus	33	500	0.25	380	29.0	9.76	TA
Hipposideros speoris	9	600	0.48	308	21.0	9.53	TA
Hipposideros armiger	50	450	0.45	252	15.0	9.30	TA
Nyctalus noctula	28	540	0.45	305	12.0	9.28	TA
Pipistrellus pipistrellus	5	650	0.45	367	16.0	9.49	TA
Pipistrellus kuhlii	6	630	0.45	355	16.5	9.49	TA
Scotophilus kuhlii	20	540	0.20	445	9.0	9.32	TA
Lasiurus borealis	11	590	0.48	302	11.7	9.27	TA
Lasiurus cinereus	28	540	0.48	277	12.0	9.24	TA
Vespertilio murinus	16	555	0.45	313	25.0	9.61	TA
Miniopterus schreibersii	10	580	0.45	327	30.0	9.71	TA
Pteropus giganteus	1100	235	0.00	235	31.4	9.59	—
Pteropus vampyrus	1000	240	0.05	233	22.6	9.44	—
Rousettus aegyptiacus	165	310	0.05	299	25.0	9.59	—
Cynopterus sphinx	50	380	0.05	368	18.5	9.55	—
Macroglossus minimus	16	450	0.00	450	18.0	9.63	—
Carollia perspicillata	17	460	0.00	460	12.0	9.46	—
Artibeus jamaicensis	45	400	0.00	400	15.0	9.50	—

B.5 Cetaceans ($n = 12$)

For cetaceans, $f_H^{avg} = (1 - p_d) f_{H,surf} + p_d f_{H,dive}$ where p_d is the dive fraction and $f_{H,dive}$ is the bradycardic dive rate [31, 32].

Table 16: Cetaceans. Clade mean $\bar{\ell} = 8.801 \pm 0.296$ ($n = 12$, dive-corrected). Corr. DA.

Species	M (kg)	$f_{\mathrm{H,surf}}$	p_{d}	$f_{\mathrm{H}}^{\mathrm{avg}}$	T (K)	L (yr)	ℓ	Src
Balaena mysticetus	100000	30	0.75	9.75	308.0	200.0	9.01	G
Balaenoptera musculus	140000	8	0.70	4.0	308.0	110.0	8.36	G
Balaenoptera physalus	60000	10	0.68	5.0	308.5	90.0	8.37	G
Megaptera novaeangliae	40000	15	0.65	7.0	308.5	95.0	8.54	G
Physeter macrocephalus	45000	40	0.65	19.0	307.0	70.0	8.84	G
Kogia breviceps	360	80	0.45	48.0	308.5	23.0	8.76	A
Hyperoodon ampullatus	7500	45	0.55	24.0	308.0	37.0	8.67	A
Orcinus orca	4000	80	0.40	53.0	309.0	90.0	9.40	A
Tursiops truncatus	190	110	0.40	74.0	309.0	40.0	9.19	A
Stenella attenuata	55	120	0.35	84.0	309.0	20.0	8.95	A
Delphinapterus leucas	1400	50	0.55	27.5	309.5	35.5	8.71	A
Monodon monoceros	1500	45	0.55	25.5	309.0	48.0	8.81	A

B.6 Birds ($n = 78$, selected entries)

Heart rates from Prinzinger et al. [29] and Clarke & Rothery [40]; lifespans from AnAge [28]. No duty-cycle correction applied ($f_{\mathrm{H}}^{\mathrm{avg}} = f_{\mathrm{H}}$). Clade mean $\bar{\ell} = 9.528 \pm 0.213$. Representative species are shown; the full list of all 78 species is available in the machine-readable data file.

Table 17: Birds (selected; $n = 78$ total). All $T \approx 311$–312 K.

Species	M (kg)	f_H (bpm)	L (yr)	ℓ	Order
Calypte anna	0.004	1200	12.0	9.88	Apodiformes
Serinus canaria	0.020	680	24.0	9.93	Passeriformes
Taeniopygia guttata	0.013	640	15.6	9.72	Passeriformes
Turdus merula	0.100	440	21.1	9.69	Passeriformes
Columba livia	0.350	190	35.0	9.54	Columbiformes
Gallus gallus	2.000	300	30.0	9.68	Galliformes
Anas platyrhynchos	1.200	190	29.0	9.46	Anseriformes
Larus argentatus	1.200	165	49.0	9.63	Charadriiformes
Diomedea exulans	9.600	100	70.0	9.57	Procellariiformes
Aquila chrysaetos	5.000	130	46.0	9.50	Accipitriformes
Bubo bubo	2.900	165	68.0	9.77	Strigiformes
Psittacus erithacus	0.400	200	73.0	9.89	Psittaciformes
Amazona ochrocephala	0.460	185	80.0	9.89	Psittaciformes
Cacatua galerita	0.840	170	80.0	9.85	Psittaciformes
Aptenodytes forsteri	30.00	75	50.0	9.29	Sphenisciformes
Struthio camelus	115	60	68.0	9.33	Struthioniformes
Fulmarus glacialis	0.800	175	67.5	9.79	Procellariiformes
Corvus corax	1.200	200	22.3	9.37	Passeriformes
Sturnus vulgaris	0.075	490	22.4	9.76	Passeriformes
Ciconia ciconia	3.700	150	48.0	9.58	Ciconiiformes

Full 78-species bird dataset available in the machine-readable data file from the corresponding author. The 20 representative species shown above span the body-mass range from 4 g to 115 kg and include both the highest ($\ell \approx 9.93$, canary) and lowest ($\ell \approx 9.05$, emu) avian values.

B.7 Reptiles — Arrhenius-corrected ($n = 17$)

f_H^{raw}: measured rate at mean field temperature T_{field}. f_H^{corr}: corrected to $T_{ref} = 310$ K via $f_H^{corr} = f_H^{raw} \exp[(E_a/k_B)(1/T_{field} - 1/T_{ref})]$, $E_a = 0.65$ eV [35].

Table 18: Reptiles. Raw mean $\bar{\ell}^{\,\mathrm{raw}} = 8.615$; corrected mean $\bar{\ell}^{\,\mathrm{corr}} = 8.929 \pm 0.301$. Corr. AQ.

Species	M (kg)	T_{field} (K)	$f_{\mathrm{H}}^{\mathrm{raw}}$	$f_{\mathrm{H}}^{\mathrm{corr}}$	L (yr)	ℓ^{raw}	ℓ^{corr}	Src
Lacerta agilis	0.015	301	45	93	12.0	8.45	8.77	Ch,U
Anolis carolinensis	0.006	302	52	106	6.0	8.22	8.52	Ch,U
Pogona vitticeps	0.350	303	42	82	10.0	8.34	8.63	Ch,U
Phrynosoma cornutum	0.035	301	48	99	7.0	8.25	8.56	Ch,U
Iguana iguana	4.000	303	40	79	20.0	8.62	8.92	Ch,U
Varanus komodoensis	65	303	28	55	30.0	8.65	8.94	Ch,U
Tupinambis merianae	2.5	302	38	77	15.0	8.48	8.78	Ch,U
Thamnophis sirtalis	0.050	300	30	62	10.0	8.20	8.51	Ch,U
Coluber constrictor	0.340	301	35	72	13.0	8.38	8.69	Ch,U
Python reticulatus	75	302	20	41	25.0	8.42	8.73	U
Boa constrictor	15	301	25	52	40.0	8.72	9.04	U
Chelonia mydas	180	300	20	42	80.0	8.93	9.25	U
Geochelone gigantea	200	298	15	33	175.0	9.14	9.48	U
Gopherus agassizii	4.5	299	22	47	80.0	8.97	9.30	Ch,U
Sphenodon punctatus	0.800	293	18	43	77.0	8.86	9.24	Ch,U
Crocodylus niloticus	400	303	25	49	70.0	8.96	9.26	Ch,U
Alligator mississippiensis	250	302	28	57	50.0	8.87	9.18	Ch,U

B.8 Amphibians — Arrhenius-corrected ($n = 9$)

Table 19: Amphibians. Raw mean $\bar{\ell}^{\,\mathrm{raw}} = 8.448$; corrected mean $\bar{\ell}^{\,\mathrm{corr}} = 8.822 \pm 0.146$. Corr. AQ.

Species	M (kg)	T_{field} (K)	$f_{\mathrm{H}}^{\mathrm{raw}}$	$f_{\mathrm{H}}^{\mathrm{corr}}$	L (yr)	ℓ^{raw}	ℓ^{corr}	Src
Rana temporaria	0.025	294	25	55	16.0	8.32	8.67	A,Ch
Rana catesbeiana	0.500	296	20	43	16.0	8.23	8.56	A,Ch
Bufo bufo	0.150	293	22	53	36.0	8.62	9.00	A,Ch
Xenopus laevis	0.200	295	20	45	30.0	8.50	8.85	A
Ambystoma mexicanum	0.300	294	18	41	25.0	8.37	8.73	A
Salamandra salamandra	0.080	290	20	49	24.0	8.40	8.79	A,Ch
Plethodon glutinosus	0.012	291	30	74	20.0	8.50	8.89	A
Necturus maculosus	0.130	288	18	46	30.0	8.45	8.86	A
Cryptobranchus alleganiensis	0.600	289	15	39	55.0	8.64	9.05	A

Dataset summary. Table 20 gives clade counts, body-mass ranges, and ℓ statistics for all eight groups ($n = 230$ total).

Table 20: Summary of the 230-species PBTE dataset. n: species count. $\bar{\ell} \pm s$: mean ± s.d. of ℓ. $\Delta\ell$: deviation from the non-primate placental baseline ($\bar{\ell}_0 = 8.995$). $^{*}p < 0.05$, $^{***}p < 0.001$ (Welch t-test vs. baseline).

Group	n	M range (kg)	$\bar{\ell} \pm s$	$\Delta\ell$	Notes
NP placentals	46	0.002–4000	8.998 ± 0.160	0 (ref.)	3 imputed f_H
Marsupials/mono.	19	0.018–30	8.933 ± 0.204	−0.062	
Primates	18	0.35–160	9.376 ± 0.125	+0.381***	
Bats	31	0.005–1.1	9.540 ± 0.163	+0.545***	duty-corrected
Cetaceans	12	55–140000	8.801 ± 0.296	−0.194	dive-corrected
Birds	78	0.004–115	9.528 ± 0.213	+0.533***	
Reptiles (corr.)	17	0.006–400	8.929 ± 0.301	−0.065	Arrhenius-corr.
Amphibians (corr.)	9	0.012–0.60	8.822 ± 0.146	−0.173	Arrhenius-corr.
All endotherms	194		9.509 ± 0.397		
Full dataset	230		9.420 ± 0.428		